A KINEMATIC MODEL TO STUDY THE DISTRIBUTION OF PRECIPITATION IN A CUMULUS UPDRAFT

by

MAN KONG YAU

S.B., Massachusetts Institute of Technology
(1971)

SUBMITTED IN PARTIAL FULFILLMENT

OF THE REQUIREMENTS FOR THE

DEGREE OF MASTER OF SCIENCE

at the

MASSACHUSETTS INSTITUTE OF

TECHNOLOGY

May, 1973

Signature of Author.....
Department of Meteorology, May 11, 1973

Certified by.....
Thesis Supervisor

Accepted by.....
Chairman, Departmental Committee
on Graduate Students

A KINEMATIC MODEL TO STUDY THE DISTRIBUTION OF PRECIPITATION IN A CUMULUS UPDRAFT

by

MAN KONG YAU

Submitted to the Department of Meteorology on May 11, 1973 in partial fulfillment of the requirements for the degree of Master of Science.

ABSTRACT

This study is concerned with the development of techniques which serve as a diagnostic tool for parameterization schemes and to provide insight into understanding the relations among air motion, microphysics, and the distribution of precipitation and radar reflectivity associated with cumulus convection. The two principle areas of investigation are: (1) the development of a three-dimensional model based on a set of continuity equations with specified air motions and microphysical parameterization; (2) the determination of the effects and importance of the roles of the microphysics and the updraft forms from one-dimensional computations.

Equations expressing the conservation of cloud and precipitation serve as the basis for the three-dimensional formulation. The form of the vertical velocity profile in a varying updraft is specified to conform to the average mass transport curve in cumulus cells derived by Austin and Houze (1973). To explore the effect of the shape and intensity of an updraft column, a constant profile with different amplitudes is also used. The motion outside the cell is assumed to be horizontal, with a convergent flow to satisfy air mass continuity superimposed on a flow around a solid cylinder in the region of the cell. The slope of the updraft is calculated from the trajectories of successive rising air parcels obeying the principle of conservation of linear momentum.

Parameterization techniques introduced by Kessler (1969) and Berry (1967,1968a,1968b) and used with exponential raindrop-size distribution falling at a single speed and also with division of precipitation water into nine different size categories each with its own fall velocity. Sensitivity tests on these microphysical parameters are performed in one-dimensional computations. The results are also applied to the interpretation of radar data.

It is found that the distribution of cloud and precipitation is relatively insensitive to the form of the autoconversion function except when unrealistically high values are used for the threshold of cloud water content needed to permit any conversion to precipitation. It is concluded that a simple linear or parabolic function is adequate for parameterization of this process.

The division of precipitation into different size and fallspeed categories as compared with the assumption of an exponential size distribution and one fall velocity is shown to be important in the formation, evolution, and distribution of precipitation. The model computations indicate a narrowing of the drop-size spectrum upward into the cell and reveals the feasibility of developing an exponential spectrum from initial narrow distributions by the accretion and coalescence processes.

The updraft profile and magnitude, especially near the cloud base, influence strongly the distribution of precipitation and subsequent evolution of the size spectrum. With a stronger updraft speed near cloud base there is a considerably greater accumulation of precipitation in the lower portion of the cloud. The characteristic cloud and precipitation profiles displayed by different updrafts point to the possibility of making some inferences regarding the shape and magnitude of the updraft column from radar-observed precipitation patterns.

A significant problem in radar measurements of precipitation is demonstrated by the computation results. Depending on the time and space evolution of the drop-size spectrum, interpretation of measured reflectivity in terms of liquid water content using Z-M relations obtained from drop-size distribution measurements at the surface may significantly over or underestimate the actual mass of precipitation present.

It is recommended that a single simple autoconversion function, the division of precipitation water into size categories and the use of an intermediate type of updraft profile(or perhaps two profiles) be used with the three-dimensional model to explore the effects on the distribution of precipitation of wind shear, sloping updrafts and moving cloud base.

Thesis Supervisor: Dr. Pauline M. Austin

Title: Senior Research Associate

TABLE OF CONTENTS

LIST OF TABLES

LIST OF FIGURES

I. INTRODUCTION

A. The general problem

The physics of cloud and the accompanying circulation have been studied almost independently in the past. In fact, not until recently has the importance in the interaction between cloud microphysical processes and dynamics in the shaping of precipitation been fully recognized. Mason (1969) emphasized this as one of today's outstanding problems in cloud and precipitation studies. He pointed out that the growth and fallout of hydrometeors was bound to have an effect on the air motion, which in turn controlled their growth and development.

Such interaction in fact begins at an early stage of cloud formation. The air motion in and around the cloud, together with the properties of the aerosols acting as condensation and freezing nuclei, determines the concentration and initial size distribution as well as the physical nature of the cloud particles. Although subsequent broadening of the size spectrum to produce precipitation is the result of collision, coalescence, and accretion, the rate and duration of such processes are nevertheless governed by the circulation, through its control on the dimension, water content and duration of the updraft column. In addition, the intensity and distribution of precipitation is often the direct result of the air motion. Conversely, the growth and evaporation of hydrometeors give rise to heat sources and heat sinks, which affect tremendously the circulation dynamics. The release of latent heat increases

the buoyancy while the drag force introduced by the falling condensate brings about an opposite effect. Thus a complicated feedback mechanism is in operation.

The realization of the importance of this interaction has resulted in the incorporation of many features of cloud microphysics into dynamic models of cumulus cells (e.g. Simpson and Wiggert (1968); Weinstein (1969); Takeda (1971)). Because of the non-linearity of the model equations, numerical methods seem to be the only means of obtaining a solution at the present time. In general, the small number of grid points involved enables one-dimensional models to include fairly complicated microphysical parameterization. However, the limitation imposed by their dimensionality excludes their use in the investigation of the interaction between ambient wind field and a convective column, whose development is to a large extent influenced by wind shear in the vertical. (Braham (1949); Newton (1963)). Moreover, the assumed top-hat profile does not allow any horizontal variation of variables. Such aspects can be studied only through models with two or three dimensions.

Observations on convective systems generally reveal a three dimensional structure of air motion. Browning (1965) analysed in detail a family of convective storms in Oklahoma. He found that the associated wind field changed sharply in the vertical both in strength and direction. Several updraft columns or cells often existed in close proximity from each other. The interweaving flow

became highly complicated. To adequately understand these natural phenomena, higher dimensional models must be used.

Numerical simulation of dynamic cloud models suffers from the drawback of providing limited insight into the underlying physics. To understand the role of a physical process, it is essential to identify the effects the process produces. The complexity of the dynamic formulation however, may preclude such interpretation. It is true that altering a physical assumption or parameterization produces a change in the outcome. But the complicated feedback mechanism linking microphysics, dynamics, and thermodynamics makes it difficult or impossible to assess to what extent such deviation is a product of a particular assumption or parameterization.

The present-generation computers also impose heavy constraints on dynamic three-dimensional numerical experiments. Due to speed and storage limitations, so far only shallow convection has been simulated. A recent attempt in this direction was the work of Steiner (1972). He successfully integrated the evolution of a three-dimensional non-precipitating buoyant element in a sheared environment. But no microphysical processes were considered.

Kinematic models can help to solve the above difficulties. Exploration of parameterization schemes to see how they affect directly the distribution of cloud and precipitation is possible without the complication of the indirect influence of associated changes in air circulation. In addition, this method of attack makes it possible to separate out certain aspects of the interaction between hydrometeors and the motion field for further investigation, thus furnishing better insight into such processes.

A further application of the kinematic approach lies in data interpretation. In comparing model computations with observations one is limited by the scarcity of observations and the difficulty of obtaining adequate ones. Radar can provide good time and space coverage of the life history of cumulus cells after the precipitation stage is reached. Hence it becomes important to be able to interpret radar observations in terms of the circulations which produce the precipitation. Kinematic models make available a means for studying more directly the extent of the information about the air motions which can be deduced from measurement of the radar reflectivity patterns.

B. Background

Kessler (1969) has made a detailed study of a kinematic model in one and two dimensions. He applied the mass continuity equation commonly used in fluid mechanics to the conservation of vapor, cloud, and precipitation. In his case, cloud was defined as condensed water that fully shares the air motion; while precipitation shares only the horizontal components of the circulation but falls relative to the air. He assumed a uniform fallspeed at any level, that of the median diameter drop. The following set of equations describes in density units the response of the water content of air to the wind and microphysical processes.

The equation for continuity of vapor and cloud is

$$\frac{\partial m}{\partial t} = \underbrace{u\frac{\partial m}{\partial x} - v\frac{\partial m}{\partial y} - w\frac{\partial m}{\partial z}}_{\text{advection effect}} + \underbrace{wG}_{\text{generation term}} + \underbrace{mw\frac{\partial \ln \rho}{\partial z}}_{\text{effect of compressibility of air}} - \underbrace{AC - CC + EP}_{\text{microphysical processes}} \quad (1)$$

where m is defined as the cloud density minus the saturation vapor density plus the actual vapor density. If when m is positive, the actual vapor density is taken as the saturation vapor density, then m is the amount of cloud. When m is negative, and the cloud content is zero, m is the amount of moisture required to saturate the air. The microphysical processes include the autoconversion of cloud to rain (AC), the collection of cloud by precipitation (CC), as well as the evaporation of hydrometeors (EP) falling in non-saturated air.

The equation for continuity of precipitation water is

$$\frac{\partial M}{\partial t} = -u\frac{\partial M}{\partial x} - v\frac{\partial M}{\partial y} - (V+w)\frac{\partial M}{\partial z} - M\frac{\partial V}{\partial z} + Mw\frac{\partial \ln \rho}{\partial z} + AC - CC - EP \quad (2)$$

where V is the relative fallspeed of the precipitation particles and M the precipitation content per unit volume of air.

To simplify the microphysics, Kessler made certain assumptions in his microphysical parameterization schemes. These are:

(1) Cloud changes to raindrops at the rate $K(m-a)$ where the magnitude of K and a may be selected to simulate various processes or rates;

(2) Precipitation particles once formed are distributed in

size according to an inverse exponential law (the Marshall-Palmer distribution) and they collect cloud particles or evaporate according to approximations to the natural accretion and evaporation processes:

(3) Change in shape of the size distribution of precipitation by virtue of differing fallspeeds within it, and by evaporation, condensation and accretion processes is omitted.

Kessler's parameterization schemes have been used widely in dynamic modelling of convective elements. However, for some applications the extent or mode in which these approximations influence the results has not been adequately explored. This study will attempt to give a clearer picture in this respect.

C. Purpose of the present study

The purpose of the present study is twofold:

(1) To develop techniques for investigating relationships among air motion, microphysical processes, and the distribution of hydrometeors, with an aim toward application of the results to the interpretation of radar observations of precipitation.

(2) To investigate the role and relative importance of the various parameters that govern the kinematics and microphysical processes in the shaping of precipitation. The result of these studies would be helpful in justifying the validity of the existing cumulus parameterization schemes or in providing insight into

better refinement in the formulation of these processes.

Specifically, the following will be carried out:

(1) Formulation of a three-dimensional kinematic model. The set of time-dependent continuity equation for cloud and precipitation will be rederived in pressure coordinates while the distinction between cloud and precipitation as defined by Kessler will be maintained. This three-dimensional formulation is important to investigate the effects on the distribution of precipitation of low level inflow, the slope of the updraft, the trajectory of the air parcels, and the movement of the cloud source. The air circulation will be specified in accordance with the present knowledge of cumulus dynamics and entrainment.

(2) Numerical experiments will be performed only for the one-dimensional case. This precludes for the time being examination of the effects of a sheared environment. Specifically the one-dimensional studies will address the effects of the nature of the autoconversion function, the vertical profile of the updraft speed and the parameterization of the raindrop sizes.

II. GENERAL DESCRIPTION OF THE MODEL

This chapter describes the development of a three-dimensional model of a cumulus updraft in a saturated environment. In a study of convective systems in New England, Austin and Houze (1972) have found that in a variety of situations including air-mass thunderstorms, cumulus cells which produce precipitation are always embedded in larger mesoscale precipitation areas. This evidence indicates that the immediate environment of such cells is usually saturated.

This saturated environment is dominated by a horizontally uniform unobstructed air flow before an updraft column makes its appearance. Although the air motion can remain constant with height, a veering and shearing of the wind in the vertical is more likely to be observed and can be prescribed in the three-dimensional model.

At an initial time the environment is disturbed by a cumulus updraft rising from a certain base level. For simplicity, the cloud is assumed to be cylindrical in shape with a constant radius at all levels, but it need not be vertical.

A vertical velocity profile is prescribed which increases with height up to some level ζ as air is entrained from the environment. Above ζ, it decreases and air is detrained. The updraft velocity when averaged over the horizontal cross-section of the cell, determines the rate of rise of the cloud top. This assumption is consistent with the requirement of air mass continuity and with

theoretical and laboratory studies on rising thermals by Levine (1965) and Saunders (1962). Their investigations have shown that the upward speed of a cloud cap is about half the maximum vertical velocity in the core below. Inside the cell, then, the cloud air moves upward while also converging toward the center of the cell. Divergent flow from the center occurs at a reglet at the cloud top as it rises and above $\frac{1}{2}$ at all times.

The rising air column interacts with the air in the environment. The former acts as a barrier to the wind field which now has to flow around the cylinder in the region of the cell. A further modification is introduced by the prescribed upward velocity. Its increase in magnitude with height demands an inflow from the surrounding region to provide for the continuity of air. This concept is similar to the one discussed by Houghton and Cramer (1951) and is termed "dynamic entrainment".

The velocity field in the environment determines the trajectory of a rising air parcel through its influence on the horizontal velocity inside the cell. It should be noted that this velocity is not the same as that of the air outside. The horizontal velocity in the updraft is determined by the conservation of linear momentum as air is entrained and mixed and by the pressure force exerted on the rising parcel by the outside air. The trajectory is important in determining the slope of the updraft. This is defined as the locus of successive air parcels rising from the cloud base. In

the event that the updraft source is stationary, the locus is identical to the trajectory. In this case a vertical wind shear results in an updraft sloping downwind while an upright cell appears when the air velocity does not vary with height. The case becomes more complicated if the source moves. The effect has been examined by Newton (1966) who noted that depending on the horizontal velocity of the source the updraft can actually slope in an upshear direction. There is practically no empirical or theorectical information regarding the manner in which the base of an updraft moves in a non-stationary atmosphere. The effect on the distribution of precipitation of varying this motion is one of the factors to be explored with the three-dimensional kinematic model.

Outside the cell region the motion is essentially horizontal with a convergent flow superimposed on a flow around a solid cylinder. The presence of small mesoscale areas around a cell indicates the absence of downward compensating current in its immediate environment, since there would be evaporation rather than enhanced precipitation if the air were undergoing subsidence.

Fig.1 depicts the situation of a sloping cell in a sheared environment. No attempt is made to incorporate the downdraft in this model. In practice the downdraft is difficult to formulate and in fact little is known about its influence and dynamics.

As the air rises, condensation following a selected moist

adiabat is assumed to take place. Although actual sounding data in convective showers reveal some deviation of the cellular temperature profile from a moist adiabatic curve, the effects are often small and as a first approximation, can be neglected. The condensed water vapor changes to cloud and precipitation by the microphysical processes. This continues to take place until the cloud top reaches its top level. At this time the updraft may be turned off and the precipitation allowed to rain out, or the updraft may be continued for any desired length of time.

The model is governed by the continuity equations formulated by Kessler. In pressure coordinates, equations (1) and (2) become

$$\frac{\partial m}{\partial t} + \frac{\partial mu}{\partial x} + \frac{\partial mv}{\partial y} + \frac{\partial m\omega}{\partial p} = -\omega G - Ac - cc \tag{3}$$

$$\frac{\partial M}{\partial t} + \frac{\partial Mu}{\partial x} + \frac{\partial Mv}{\partial y} + \frac{\partial M\omega}{\partial p} + \frac{\partial M\dot{p}}{\partial p} = Ac + cc \tag{4}$$

The m and M now refer to mixing ratios of cloud and precipitation; ω denotes the vertical velocity in mb sec^{-1} while $\dot{p}$ is the fallspeed of precipitation particles in the same unit.

Using the continuity equation

$$\frac{\partial u}{\partial x} + \frac{\partial v}{\partial y} + \frac{\partial \omega}{\partial p} = 0 \tag{5}$$

(3) and (4) can be rewritten as

$$\frac{\partial m}{\partial t} + u\frac{\partial m}{\partial x} + v\frac{\partial m}{\partial y} + \omega\frac{\partial m}{\partial p} = -\omega G - Ac - cc \tag{6}$$

$$\frac{\partial M}{\partial t} + u\frac{\partial M}{\partial x} + v\frac{\partial M}{\partial y} + \omega\frac{\partial M}{\partial p} = Ac + cc \tag{7}$$

The precipitation water can be broken up into different size categories with their own fall velocities. Each group then will be governed by its evolution equation having the same form as (7).

The formulation of the equations for the motion field and the microphysical processes are in chapters III and IV. The aspects to be explored with the model are the effect on the distribution of precipitation and radar reflectivity produced by:

(a) Varying the assumed updraft profile

(b) Using different functions for rate of conversion of cloud to precipitation

(c) Treating the precipitation as a single quantity with a single fall velocity and using a number of size categories with different fall velocities

(d) Varying the motion of the inflow region at cloud base (thereby simultaneously affecting the updraft slope)

(e) Varying the wind shear.

First three will be explored with one-dimensional computation.

III. FORMULATION OF THE MODEL-KINEMATICS

A. Definition of quantities

The kinematics deals with the specification of the horizontal and vertical motion field both inside and outside the updraft column. The slope of the cell (the updraft region at any instant) is determined by the trajectories of individual parcels or wafers of rising air in combination with the motion of the cell base or source of rising air. The motion of the cell is the same as that of the source. In order to study the effect on the distribution of precipitation particles by a moving source, all horizontal motions are defined relative to $\vec{V}_s$, the velocity of the moving cloud base. Hence in the numerical computations, the cell will be standing still in an x,y,p coordinate system.

The various quantities that enter into the equations are defined as follows:

$\mathcal{M}(p)$ = average mass transport per unit area through level p in g m^{-2}

$\omega(r,p,t) = \omega(r,p)\,T(t)$
=time-dependent updraft velocity in mb sec^{-1}

$\omega(r,p)$ = time-independent part of the updraft velocity in mb sec^{-1}

$\bar{\omega}(p)$ = horizontal average of $\omega(r,p)$

$\omega_{max}(p)$ = maximum value of $\omega(r,p)$ at the cell center

P_T = cloud top level in mb

P_B = cloud base in mb

r = radial distance from the center (x_0, y_0) of the cell and is equal to $[(x-x_0)^2 + (y-y_0)^2]^{\frac{1}{2}}$

r_0 = radius of the updraft, constant at all levels

$t_i(p)$ = time when updraft reaches level p in seconds.

$t_f(p)$ = time when updraft is assumed to cease

$T(t)$ = time-dependent part of $\omega(r, p, t)$

$\vec{V}'(p)$ = horizontal velocity of parcel wafer

u, v = x,y components of any vector velocity

$\vec{V}_e(p) = \vec{V}_i(p) + \vec{V}_{cy}(p)$
= total horizontal velocity outside the cell region, in m sec^{-1}

$\vec{V}_i(p)$ = convergent part of $\vec{V}_e$, m sec^{-1}

$\vec{V}_{cy}(p)$ = component of $\vec{V}_e(p)$ that flows around a solid cylinder, m sec^{-1}

$\vec{V}_{eo}(p)$ = horizontal velocity before the appearance of the updraft, m sec^{-1}

$\vec{V}_c(p)$ = horizontal velocity inside the cell region, m sec^{-1}

ζ = pressure level at which $\bar{\omega}(p)$ is a maximum

θ = azimuthal angle

ρ_{air} = density of air in kg $mb^{-1}m^{-2}$

x_o, y_o = position of the cell center, a function of p only.

B. Specification of vertical velocity

The form for $\bar{\omega}(p)$ is selected to conform to the one used by Austin and Houze (1973). They developed this formulation in accordance with the present knowledge of cumulus dynamics as well as recent theorectical and experimental results on entrainment rates. However, in this time-dependent model it is no longer feasible

to assume that $\bar{\omega}(p)$ takes on the same shape as the total mass transport $m(p)$. Therefore a parametric form of $\bar{\omega}(p)$ is first specified. The parameters are then adjusted so that the total cellular transport given by

$$(t_i(P_T) - t_i(p))\,\bar{\omega}(p)\,\rho_{air} = m(p) \tag{8}$$

fits that of Austin and Houze's.

To solve (8) for $m(p)$ the form of $\bar{\omega}(p)$ is written as follows:

$$\bar{\omega}(p) = A\left[a'(P - P_T)^m e^{-b(p-P_T)^n}\right] \tag{9}$$

In (9), A is the amplitude of the updraft; a' is a normalization constant to normalize the maximum value of the quantity in brackets to one; b determines the level ζ where the velocity is a maximum: m and n are constants.

In all the computations, the level at which ζ is a maximum is set at

$$\zeta = P_B - 0.2(P_T - P_B) \tag{10}$$

then b is expressed by

$$b = \frac{m}{n(0.2(P_T - P_B))^n} \tag{11}$$

Using

$$t_i(p) = \int_{P_B}^{p} \frac{dp}{\bar{\omega} p}\ , \tag{12}$$

$$t_i(P_T) = \int_{P_B}^{P_T} \frac{dp}{\bar{\omega}(p)} \tag{13}$$

and by manipulating with the constants m and n, it was found that a best fit for the shape of $m(p)$ gives $m = 0.27$ and $n = 2$. The resulting graphs for $\bar{\omega}$ and $m(p)$ are shown in figures 2 and 3. Some computations are made with $\bar{\omega}(p)$=constant in which case $m(p)$ has the form shown by

the dotted line.

A top-hat profile in which the vertical velocity is constant at any level was first considered and was used in the one-dimensional computations. However, with the finite difference scheme used in the computations, velocity discontinuities at the cell boundary would cause advection of cloud into clear air. To eliminate such difficulty, a parabolic profile is used instead,

$$\omega(r,p) = \frac{\omega_{max}(p)}{r_0^2}(r-r_0)^2 \tag{14}$$

In terms of $\bar{\omega}(p)$, which is prescribed, this becomes

$$\omega(r,p) = 6\frac{\bar{\omega}(p)}{r_0^2}(r-r_0)^2 \tag{15}$$

The time-dependent part of the vertical velocity is governed by a simple step-like function $T(t)$.

$$T(t) = \begin{cases} 1 & t_i(p) \leq t \leq t_i(p_T) \\ 0 & \text{otherwise} \end{cases} \tag{16}$$

At any level the updraft must begin at $t_i(p)$ the time the cloud top reaches that level. The termination time has been set at $t_i(p_T)$ in order to avoid the problems associated with increasing the cloud radius at the top as air continues to rise in the updraft. However, the effect of varying the updraft duration is one aspect which should ultimately be explored with the kinematic model.

C. Specification of horizontal velocity

The horizontal velocities are specified in two separate regions denoted by $\vec{V}_c$ inside the cell and $\vec{V}_e$ in the environment. All motions are defined relative to the source velocity $\vec{V}_s$ as

pointed out at the beginning of this section

Inside the cell: $r \leq r_0$

In a circular wafer of radius r and depth Δp inside the updraft column, the net mass of air transported out of the wafer must be balanced by convergent flow towards the center. If $V_i(p)$ is the radial inflow to give such a balance, then

$$2\pi r\, V_i(p) = \frac{\partial}{\partial p}\int_0^{2\pi}\int_0^{r} \omega(p,r)\, r\, dr\, d\theta \tag{17}$$

Using equation (15) and integrating (17), the x and v components of $\vec{V_c}$, namely

$$u_c = -V_i \cos\theta \tag{18}$$

and

$$v_c = -V_i \sin\theta \tag{19}$$

turn out to be

$$u_c = -\frac{6}{r_0^2}\frac{\partial \bar{\omega}}{\partial p}\left[\frac{r^3}{4} - \frac{2r_0 r^2}{3} + \frac{r_0^2 r}{2}\right]\frac{x-x_0}{\sqrt{[(x-x_0)^2+(y-y_0)^2]}} \tag{20}$$

$$v_c = -\frac{6}{r_0^2}\frac{\partial \bar{\omega}}{\partial p}\left[\frac{r^3}{4} - \frac{2r_0 r^2}{3} + \frac{r_0^2 r}{2}\right]\frac{(y-y_0)}{\sqrt{(x-x_0)^2+(y-y_0)^2}} \tag{21}$$

Outside the cell: $r > r_0$

The total horizontal flow in this region is the sum of a convergent component and a part which represents the velocity field deformed by a solid cylinder. In the previously defined notation

$$\vec{V_e} = \vec{V_i} + \vec{V_{cy}} \tag{22}$$

The relation between the undisturbed flow $\vec{V_{e0}}$ before the appearance of the cell and $\vec{V_{cy}}$ has been worked out in many books on fluid mechanics (e.g. Milne-Thomson,1968). The results are

$$u_{cy} = u_{eo} - (u_{eo} + 2v_{eo}) r_o^2 \left\{ \frac{(x-x_o)^2 - (y-y_o)^2}{[(x-x_o)^2 + (y-y_o)^2]^2} \right\} \tag{23}$$

$$v_{cy} = v_{eo} - (v_{eo} + 2u_{eo}) r_o^2 \left\{ \frac{(x-x_o)^2 - (y-y_o)^2}{[(x-x_o)^2 + (y-y_o)^2]^2} \right\} \tag{24}$$

For the convergent part of $\vec{V}_e$, a similar procedure to the in-cell case shows

$$u_i = -\frac{1}{2} r_o^2 \frac{\partial \bar{\omega}}{\partial p} \frac{(x-x_o)}{(x-x_o)^2 + (y-y_o)^2} \tag{25}$$

$$v_i = -\frac{1}{2} r_o^2 \frac{\partial \bar{\omega}}{\partial p} \frac{y-y_o}{(x-x_o)^2 + (y-y_o)^2} \tag{26}$$

D. Slope of the cell

The trajectory of a rising air parcel through the updraft is determined by the position of the cell center at successive levels. If the pressure force effect is neglected, conservation of linear momentum between the rising and entrained air demands

$$\bar{\omega}(p_B)\, \vec{V}_e(p_B) + \int_{p_B}^{p} \frac{\partial \bar{\omega}(p)}{\partial p}\, \vec{V}_e(p)\, dp = \bar{\omega}(p)\, \vec{V}'(p) \tag{27}$$

and

$$\vec{V}'(p) = \frac{\bar{\omega}(p_B)}{\bar{\omega}(p)} \vec{V}_e(p_B) - \frac{1}{\bar{\omega}(p)} \int_{p_B}^{p} \frac{\partial \bar{\omega}(p)}{\partial p} \vec{V}_e(p)\, dp \tag{28}$$

Equation (28) applies to all levels below ζ. Above ζ the absence of entrainment indicates that $\vec{V}'(p)$ and $\vec{V}'(\zeta)$ be equal.

With $\vec{V}'(p)$ and $\bar{\omega}(p)$ known, the position of x_o and y_o for any assumed wind field can be calculated by the following relations

$$dx = u'\, dt \tag{29}$$

$$dy = v'dt \tag{30}$$

and

$$dp = \bar{\omega}_q v dt \tag{31}$$

In the development of the kinematics, two important features have been left out, namely the drag force and the downdraft. The magnitude of the drag force effect is not really known.But Austin and Houze(1973) have made a computation which could serve as a guideline for incorporating it into a kinematic model. The mechanism of the downdraft however, is still poorly understood, and is therefore omitted from the present formulation. But it can be added if it is found desirable to study its influence in future computations.

IV. FORMULATION OF THE MODEL- MICROPHYSICAL PARAMETERIZATION

A. Parameterization schemes which have been used.

(1) Autoconversion

Autoconversion is a simplified treatment of the formation of precipitation by the complicated mechanisms of aggregation of cloud droplets into precipitation particles. This idea was introduced by Kessler (1969) who assumed a simple linear relation of the form

$$\frac{dM}{dt} = K(m-a) \tag{32}$$

The parameter K is the reciprocal of the 'conversion time' of the cloud water. Kessler chose K as 10^{-3}sec^{-1} to be consistent with a cloud lifetime of about 1000 seconds. The a denotes a threshold cloud water content at which conversion is hypothesized to commence.

Another formulation of the autoconversion process has been developed by Berry (1967,1968a,1968b). He derived his autoconversion equation from a stochastic model of cloud growth in which some of the larger cloud droplets may undergo an above-average number of chance collisions to produce a fast spread of the spectrum. The emphasis here is on all combinations of droplets that are able to coalesce, the probability of each coalescense, and the changes in these probabilities after each coalescence. Berry performed a number of numerical experiments with specified cloud spectra at the base and observed the subsequent evolution of the size distribution. He then calculated the autoconversion rate as the

ratio of the liquid water content to the time required for the center of mass of water to pass a certain threshold between cloud and precipitation. His formula for a 200μ threshold is

$$\frac{dM}{dt} = \frac{m^2}{60\left(5 + \frac{0.0366}{m}\frac{N_b}{D_b}\right)} \qquad (33)$$

where N_b = initial drop concentration per unit volume at the cloud base

D_b = relative dispersion due to the condensation spectrum

$$= \frac{\text{standard deviation of droplet radius}}{\text{mean droplet radius}}$$

Autoconversion rates for different cloud types can be modelled by Berry's formula. Measurements by Squires (1958), and MacCready and Takeuchi (1968) have shown that maritime and continental clouds can be distinguished by the differences in N_b and D_b. Representative values are

	Continental	Maritime
N_b	2000 cm^{-3}	50 cm^{-3}
D_b	0.146	0.366

(2) Terminal velocity of precipitation particles

The terminal velocity of water drops falling through the atmosphere is determined by the shape and diameter of the drops, as well as other circulation effects. Stoke's law for the resistance to motion of a rigid sphere moving in a viscous fluid approximates only the terminal velocity of very small drops. But no analytic relation is presently available to describe the fall velocity of

water drops in the whole size spectrum. Therefore it becomes necessary to rely on empirical data. Fairly extensive measurements for sea level pressures have been made (e.g.Gunn and Kinzer, 1949), while measurements by Davis reported by Best (1950) include observations at reduced pressures as well. Davis' data when reduced to pressure coordinates is listed in tables 4.1 and 4.2.

Table 4.1

I.C.A.N. Standard Atmosphere

P(mb)	$\dot{P}/\dot{P}_o$
1013	1
900	.944
790	.885
700	.831
600	.770
507	.706
420	.642

where $\dot{P}_o$ represents the terminal velocity at 1013 mb.

Table 4.2

Terminal velocity at 1013 mb, 20°C.

$\dot{P}_o$ (mb sec^{-1})	D (cm)
-0.117	0.025
-0.234	0.050
-0.350	0.070
-0.470	0.100
-0.580	0.130
-0.700	0.175
-0.820	0.225
-0.930	0.300
-1.050	0.450

A curve which fits the data well is given by:

$$\dot{P} = \frac{1}{\sqrt{1013}} \dot{P}_0 \sqrt{P} \tag{34}$$

$$D = 0.0037 \dot{P}_0^2 \tag{35}$$

where P is in mb and D in meters.

Combining (34) and (35), a relation of the terminal velocity in terms of the diameter and pressure results

$$\dot{P} = \left(\frac{P}{1013}\right)^{\frac{1}{2}} \left(\frac{D}{0.0037}\right)^{\frac{1}{2}} \tag{36}$$

Equation (36) will be used in actual computations instead of the terminal velocity (V) relation given by Kessler where $V = -k' \exp\left(\frac{kz}{2}\right) D^{\frac{1}{2}}$, with k' and k being constants.

(3) Particle size distribution

Kessler assumed that the precipitation particles follow the Marshall-Palmer relation(1948),

$$N = N_0 e^{-\lambda D} \tag{37}$$

and derived expressions of λ and D_0, the median volume drop diameter, in terms of M. N_0, the drop density corresponding to a zero diameter is taken as a constant.

Takeda (1971) used seven particle size categories ranging from 1μ to 3000μ. Equations were developed to describe the evolution of the number of drops in each group by the changes brought about by condensation, collection, and water drop breakup. His scheme condenses water vapor on all size categories.

Cloud-droplet spectrum equations of a similar nature have

been used by Arnason and Greenfield (1972) in a numerical simulation of moist convection. Their study however, did not include the rain stage.

(4) Collection of cloud

The actual process of precipitation growth by collection of cloud is complicated. However the cloud water collected by a precipitation particle in time Δt is taken to be the mass of cloud droplets contained in the volume swept out by the falling drop, suitably modified by the collection efficiency E_c. Then for one drop with mass m_i and diameter D_i'

$$\frac{\delta m_i}{\delta t} = \frac{\pi}{4} D_i' E_c \dot{p}_i m \rho_{air} \tag{38}$$

ρ_{air} has the unit kg m^{-2}mb^{-1}.

For the Marshall-Palmer distribution, the growth of the whole spectrum is then just the integral over all sizes,

$$\frac{dM}{dt} = \int_0^\infty \frac{\pi}{4} D^2 E_c \dot{p} m \rho_{air} N_0 e^{-\lambda D} dD \tag{39}$$

With appropriate values of λ and $\dot{p}$, the result turns out to be

$$\frac{dM}{dt} = C E_c m p^{\frac{1}{2}} N_0^{\frac{1}{8}} M^{\frac{7}{8}} \rho_{air} \tag{40}$$

where C is a constant and E_c is the collection efficiency of precipitation particles for cloud drops. Equation (40) has been worked out by Kessler in density units and has been used by Simpson and Wiggert (1968) and Ogura (1971) in one-dimensional cloud models.

For assumptions of different drop-size categories, the

cloud collection equation for one drop is the same as (38) except that a representative mean diameter $\bar{D}_i$ is used instead of D'_i. Then the growth for N_i drops in the i^{th} category is

$$\Delta M_i = N_i \left(\frac{\pi}{4} \bar{D}_i^{'2} \dot{p}_i \, m \, \rho_{air} E_c\right) \Delta t = CC_i \tag{41}$$

with

$$N_i = M_i \Big/ \left(\frac{\pi}{6} \bar{D}_i^{'3} \rho_{water}\right) \tag{42}$$

(5) Distribution of reflectivity

The use of radar in the measurement of precipitation requires knowledge of the distribution of particle sizes in order to relate the rainfall rate R or rain water content M to the radar reflectivity factor Z. A number of empirical relations between these quantities have been deduced from measurements of drop size distributions at the ground. Since Z is a function of the size spectrum, different distributions must exist in different storms, different geographic locations, and possibly different stages of development of a convective system. Furthermore, it seems reasonable to believe that the size distribution is not uniform in the vertical. The Marshall-Palmer distribution is based on a large number of measurements in various situations, but all made at the ground level.

Kessler derived his reflectivity equation from the assumed Marshall-Palmer(MP) distribution. Using the relation existing between λ, N_o, and M, and integrating over the sixth power of the diameter for the whole spectrum, he arrived at an expression between Z, N_o and M given as

$$Z = 3.2 \times 10^9 \, N_o^{-.75} \, M^{1.75} \tag{43}$$

For parameterization which employs drop size categories, the reflectivity factor, defined as the sum of the product of the number of drops per unit volume and the sixth power of the mean diameter in each category, is computed as

$$Z = \sum_i N_i \bar{D}_i \tag{44}$$

B. Parameterization schemes to be used in present computation

It is recognized that parameterization schemes represent at best a crude approximation to the natural processes. It is unrealistic to assume that once precipitation particles are formed they will immediately conform to a certain exponential distribution in size, also in precipitation all particles at the same location do not fall with one and only one fall velocity. Moreover, the fast broadening of size spectrum from that of cloud to surface precipitation indicates the importance of differential fall velocities in the shaping of a distribution. It becomes necessary then to set up a scheme which simulate more realistically the growth of cloud and precipitation through the accretion process. Comparison of results with different schemes will determine how much simplification is acceptable for different computations. Furthermore, such scheme will be valuable for the study of the space and time evolution of the drop-size distribution, measurements of which are presently difficult to obtain.

The scheme to be used in the computation divides the precipitation particles into nine diameter categories, each having its own

terminal velocity. The division is based on the fall velocities with each category increasing by 1 m sec^{-1} at the surface. The third column of table 4.3 contains this increment converted to mb sec^{-1}. Corresponding drop diameters are also given in that table.

Table 4.3

CATEGORY	FALLSPEED AT SURFACE m sec^{-1}	mb sec^{-1}	RANGE OF DIAMETER D_i-D_{i-1} (cm)	MEAN DIAMETER $\bar{D}_i$ (cm)	SPREAD OF DIAMETER ΔD
1	1	-0.11	0.035<	0.0175	0.035
2	2	-0.23	0.035-0.060	0.0475	0.025
3	3	-0.35	0.060-0.085	0.0725	0.025
4	4	-0.46	0.085-0.115	0.1000	0.030
5	5	-0.58	0.115-0.155	0.1350	0.040
6	6	-0.70	0.155-0.200	0.1775	0.045
7	7	-0.82	0.200-0.260	0.2310	0.060
8	8	-0.93	0.260-0.345	0.3025	0.085
9	9	-1.05	>0.345	0.3950	0.100

(1) Condensation

A moist adiabat is chosen to represent the temperature distribution in the cell column. The $\theta_e = 314.6^{\circ}$ curve is selected to conform to a temperature of about $15^{\circ}C$ at the surface. The rate of condensation given by

$$\omega \frac{\partial Q_s}{\partial p} = \omega G \tag{45}$$

where Q_s is the saturation mixing ratio, can be fitted by a generating function of the following form

$$G = \left[0.018 - (9.5 - p/100)^3 \right] 0.000068 \tag{46}$$

This curve is shown in fig.4.

It is assumed that condensation is responsible only for the growth of cloud droplets. In actual cases, precipitation particles do grow by condensation. The rate of growth in terms of fractional increase in mass, however, is inversely proportional to the square of the diameter. Therefore with comparable water content in cloud and precipitation, the cloud droplets will accumulate the major portion of the condensed moisture, and a neglect of this effect on rain drops is not expected to produce appreciable changes in the result.

(2) Autoconversion

The autoconversion process is assumed to produce rain only in the smallest diameter category. These small drops then grow by collecting cloud particles and part of the precipitation content is transferred to a higher group. Both Kessler's and Berry's formulations will be used and the effects of using different ones will be explored. A comparison of Berry's equation for continental

and maritime cloud and Kessler's equation for $K = 10^{-3}$ sec, $\alpha = 0.5$ g kg^{-1} are plotted in fig. 5.

(3) Development of drop size distribution

Distribution of precipitation into the various drop size categories progresses by a sequence which can be illustrated. In the diagram below, the top line shows that cloud water content is increased by condensation and depleted by autoconversion and accretion.

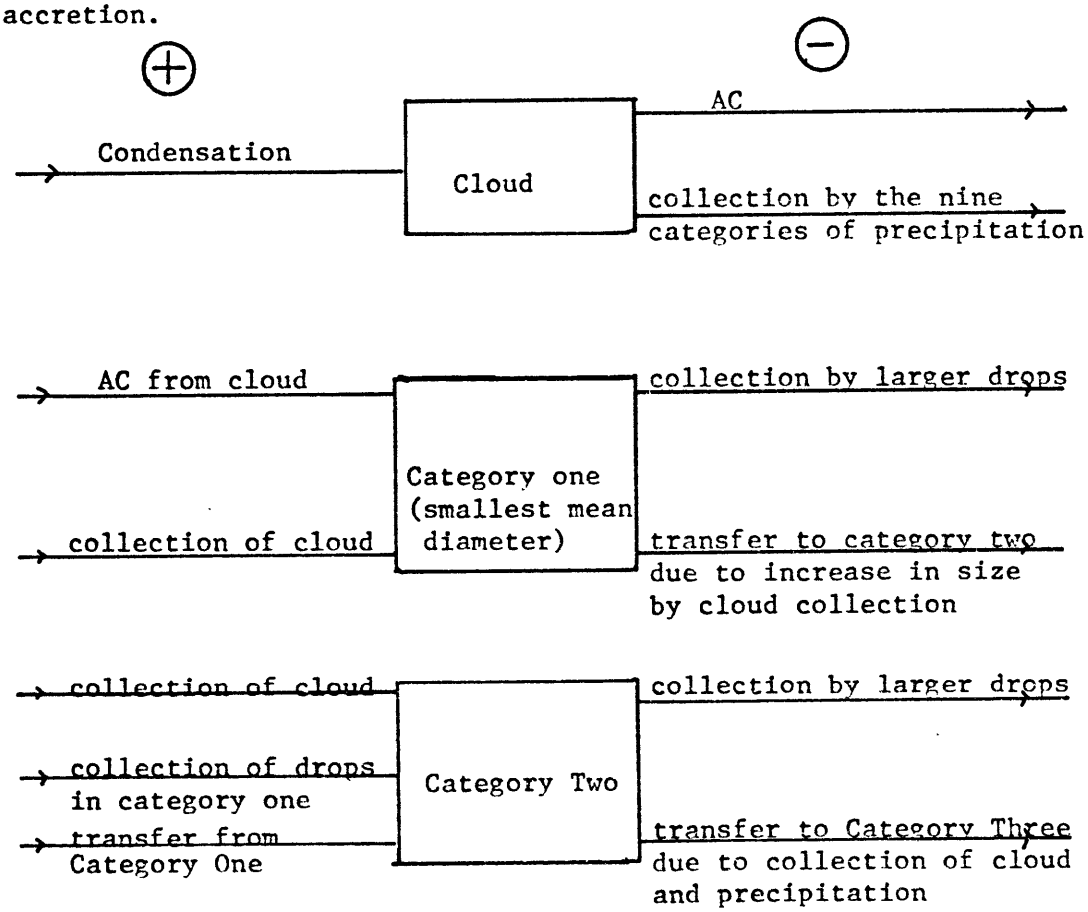

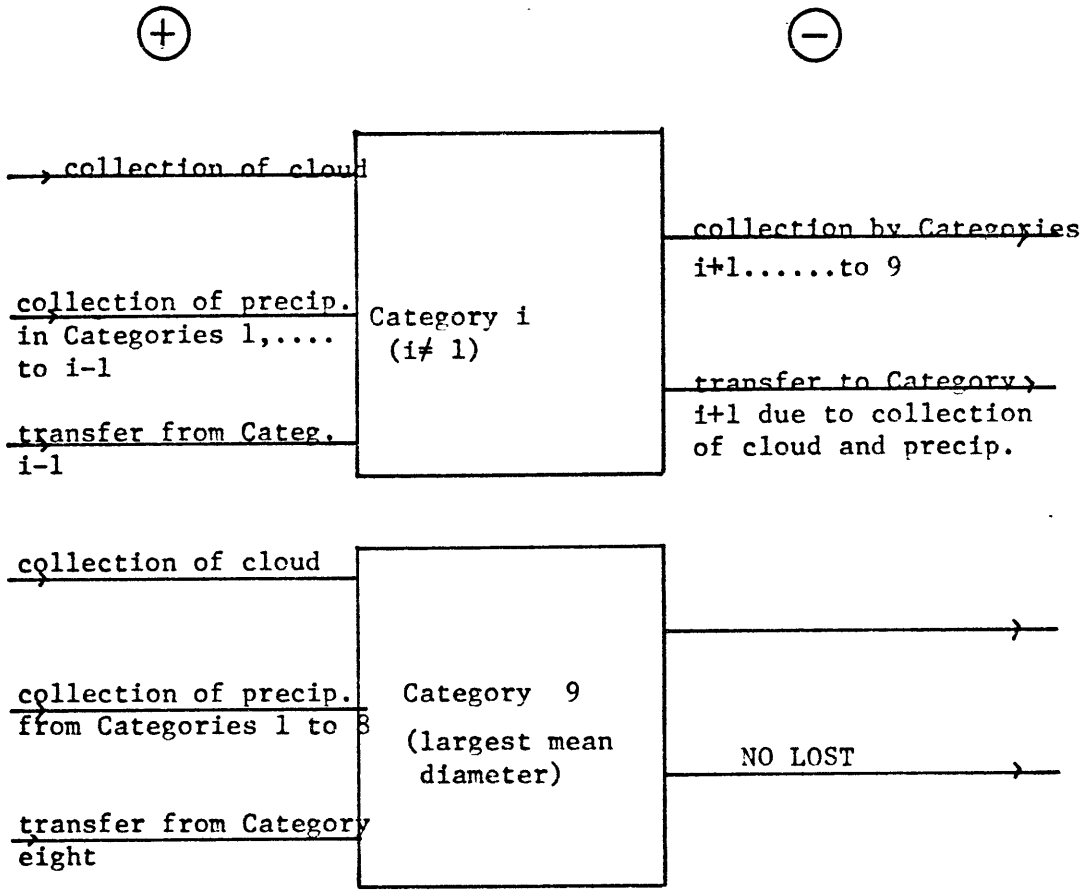

The budget of the precipitation in category i is described here. The more restricted cases of categories 1 and 9 follow a similar reasoning.

The positive budget includes

(i) Collection of cloud

(ii) Collection of precipitation in categories 1 to i-1

(iii) Transfer from category i-1 because of some drops growing beyond the threshold;

and the negative budget consists of

(i) Collection by larger drops in categories i+1 to 9

(ii) Transfer to category i+1

Positive Budget

(i) For computing the collection of cloud and small precipitation particles it is assumed that M_i is composed of N_i drops of mean diameter $\bar{D}_i$. Therefore the collection of cloud is governed by equation (41).

(ii) The increase in mass due to collection of smaller raindrops is proportional to the mass of precipitation in the swept-out volume. The proportionality constant can be considered as the collection efficiency.

Mathematically

$$\Delta M_i = N_i \pi r_i^2 \sum_{j<i} (\dot{p}_i - \dot{p}_j) M_j E_j \left(\frac{r_i + r_j}{r_i}\right)^2 \qquad (47)$$

The collection efficiency E_j in (47) is defined as

$$E_j = \frac{y_c^2}{(r_i + r_j)^2} \qquad (48)$$

where y_c is the critical impact parameter.

It is recognized that the continuous collection formula is not applicable over the entire range for raindrops. However, the more important collection is larger drops collecting the numerous small ones since the differential fall velocities are large and for this part the continuous function should be a good approximation.

(iii) For computing the transfer from category i-1, bounded by D_{i-1} and D_i, it is assumed that within each category, the mass

of precipitation is distributed uniformly over its diameter range. The drops in the $i-1^{th}$ category increase in size by collecting cloud droplets and capturing precipitation particles of a smaller size. The result of their growth will then transfer part of the water into category i.

Let D_{i-1} and D_i be the upper and lower boundaries of the $i-1^{th}$ category and $\bar{D}_{i-1}$ the mean drop diameter. For a time interval and given cloud and precipitation contents, a diameter D_j can be found between D_{i-1} and D_i such that $D_j + \delta D = D_i$. Schematically this resembles the following.

In time Δt, drops with diameter $\geq D_j$ will be transferred into category i by collection of cloud and precipitation particles. The fractional mass of precipitation transferred F is

$$F = \frac{\delta D}{D_i - D_{i-1}} \tag{49}$$

where

$$\delta D = \delta D_c + \delta D_p \tag{50}$$

δD_c is the change due to collection of cloud and δD_p that due to collection of rain. These changes are computed for the average drops in the interval.

From equation (38) it follows that

$$\delta D_i = \frac{m \dot{p}_{i-1} E_c \Delta t}{2} \frac{\rho_{air}}{\rho_{water}} \tag{51}$$

and

$$\delta D_p = \frac{1}{2} \Delta t \frac{\rho_{air}}{\rho_{water}} \sum_{j<i-1} (\dot{p}_{i-1} - \dot{p}_j) M_j E_j \left(1 - \frac{r_j}{r_{i-1}}\right)^2 \tag{52}$$

Negative Budget

A completely analogus derivation specifies the negative budget. The collection by categories i+1 to 9 is

$$\sum_{\ell>i} N_\ell \pi (Y_\ell + Y_i)^2 (\dot{p}_\ell - \dot{p}_i) M_i E_i \rho_{air} \tag{53}$$

while F' the total fractional transfer to category i+1 is given by

$$F' = \frac{\delta D_c' + \delta D_p'}{D_{i+1} - D_i} \tag{54}$$

with $\delta D_c'$ and $\delta D_p'$ computed for the mean drop diameter in the i^{th} category.

This chapter, together with the kinematics specified in chapter III give a complete formulation of the model in three dimensions. The breaking up of water drops has not been incorporated. Its significance will be explored in future computations.

V. ONE-DIMENSIONAL NUMERICAL EXPERIMENTS AND RESULTS

A. One-dimensional formulation

The numerical experiments for the one-dimensional model are described here. In particular, the equations are set out in their finite difference form. The choice of the various parameters which affect the formation and distribution of cloud and precipitation is explained.

(1) Summary of equations

For parameterization which divides the precipitation into drop size categories, each of these is governed by its own evolution equation. Hence for cloud

$$\frac{\partial m}{\partial t} + \frac{\partial m\omega}{\partial p} = B(m) \tag{55}$$

and for precipitation

$$\frac{\partial}{\partial t}\begin{Bmatrix} M_1 \\ \vdots \\ M_i \\ \vdots \\ M_q \end{Bmatrix} + \frac{\partial}{\partial p}\begin{Bmatrix} M_1(\omega+\dot{p}_1) \\ \vdots \\ M_i(\omega+\dot{p}_i) \\ \vdots \\ M_q(\omega+\dot{p}_q) \end{Bmatrix} = \begin{Bmatrix} B_1(M) \\ \vdots \\ B_i(M) \\ \vdots \\ B_q(M) \end{Bmatrix} \tag{56}$$

where M_i and $\dot{P}_i$ denote respectively the mass and the fallspeed of precipitation particles in the i^{th} category.

The right hand side of the equations represents the sources and sinks. They have the form

$$B(m) = m\frac{\partial\omega}{\partial p} - \omega G - Ac - \sum_{i=1}^{q} CC_i \tag{57}$$

$$B_i(M) = M_i\frac{\partial\omega}{\partial p} + CC_i + {}_{i-1}T_i - {}_{i}T_{i+1} \tag{58}$$

CC_i is the collection of cloud by the i^{th} group. The $_{i-1}T_i$ term, which represents the mass transferred from the $i-1^{th}$ to the i^{th} category, is given by

$$\begin{aligned} {}_{i-1}T_i &= M_{i-1}F \quad , \quad i \neq 1 \\ {}_{i-1}T_i &= AC \quad , \quad i = 1 \end{aligned} \tag{59}$$

Kessler's parameterization for precipitation with only one fall velocity is a special case of equation(56). In this case there is only one equation for precipitation and $\dot{p}_i$ is replaced by the fallspeed of the median drop.

(2) Finite difference formulation

The finite difference form of (55) and (56) has been formulated by Kessler and Newburg (1969). The form is

$$m_\ell^{n+1} = 0.5(m_{\ell+1}^n + m_{\ell-1}^n) - 0.5\frac{\Delta t}{\Delta p}\left(\omega_{\ell-1}^n m_{\ell-1}^n - \omega_{\ell+1}^n m_{\ell+1}^n\right) + 0.5\Delta t\left[B(m)_{\ell-1}^n + B(m)_{\ell+1}^n\right] \tag{60}$$

$$M_\ell^{n+1} = 0.5(M_{\ell+1}^n + M_{\ell-1}^n) - 0.5\frac{\Delta t}{\Delta p}\left((\dot{p}+\omega)_{\ell-1}^n M_{\ell-1}^n - (\dot{p}+\omega)_{\ell+1}^n M_{\ell+1}^n\right) + 0.5\Delta t\left[B(M)_{\ell+1}^n + B(M)_{\ell-1}^n\right] \tag{61}$$

Here $m_\ell^n = m(\ell\Delta p, n\Delta t)$, Δt and Δp are respectively the time and space steps which have the values of 10 seconds and 20 mb in this study. The cloud base condition is

$$m_{base}^{n+1} = m_{base}^n + \Delta t\left[B(m)_{base}^n - \left(m\frac{\partial w}{\partial p}\right)_{base}^n\right] \tag{62}$$

Below the base

$$M_\ell^{n+1} = M_\ell^n - \frac{\Delta t}{\Delta p}\left[M_\ell^n(\omega+\dot{p})_\ell^n - M_{\ell+1}^n(\omega+\dot{p})_{\ell+1}^n\right] + B(M)_\ell^n \tag{63}$$

and

at the top as it rises

$$m_{top}^{n+1} = m_{top}^n - \frac{\Delta t}{\Delta p}\left(m_{top-1}^n \omega_{top-1}^n - m_{top}^n \omega_{top}^n\right) + \Delta t\, B(m)_{top}^n \tag{64}$$

The stability criteria for this set of equations is governed by

$$\Delta\tau \leq \frac{0.8\,\Delta p}{|\omega+\dot{p}|_{max}} \qquad (65)$$

$$\text{or} \quad \Delta t \leq \frac{.8\,\Delta p}{\omega_{max}}$$

(3) The choice of parameters

The various constants used and the tests performed on the parameterization schemes are summarized in table 5.1.

The choice of the autoconversion parameters is guided by several criteria. The values of **K** are selected to approximate the slope in Berry's autoconversion formula for the continental and maritime cloud. Besides three constant values for the threshold, two linear profiles are also used. a(inc) has zero value at the cloud base and increases to 2 g kg^{-1} at the top. a(dec) gives the opposite effect.

Hockings (1959), Shafrir and Neiburger (1963), Davis and Sartor (1967) and others have calculated collision efficiencies for water drops of various sizes. A cloud collection efficiency of 0.8 is picked to conform to these findings. The efficiency for precipitation drops however, varies over a wide range. It is small for large drops collecting very small ones, but the wake capture effect for drops of comparable sizes can result in an efficiency exceeding unity. For simplicity, a value of one is used.

TABLE 5.1

PROCESS	PARAMETER	MEANING	VALUE	
			SINGLE FALL VELOCITY CASE	CASE FOR DIFFERENCE SIZE CATEGORIES
Autoconversion	K	autoconversion rate	10^{-3} and 6.2×10^{-3} sec^{-1}	0.5×10^{-3}, 10^{-3}, 6.2×10^{-3} sec^{-1}
	a	constant autoconversion threshold	0.5, 1, 2 g kg^{-1}	same
	a(dec) a(inc)	variable autoconversion threshold	$0.004\ (P-P_T)$ g kg^{-1} $2-0.004\ (P-P_T)$ g kg^{-1}	same
Collection of cloud	E_c	collection efficiency	0 or 0.8	same
	N_o	Marshall-Palmer intercept	10^7	not used
Collection of precipitation	E	collection efficiency	not used	1

TABLE 5.1 cont.

Varying updraft	A	amplitude	-0.34 mb sec^{-1}	same
Constant updraft		amplitude	-0.22, -0.34, and -0.5 mb sec^{-1}	same
	P_T	cloud top	420 mb	same
	P_B	cloud base	900 mb	same

Based on a number of observational results, Austin and House (1973) have used a maximum updraft velocity of 5 m sec^{-1} for cells with a vertical extent of about 7 km. The amplitude of the varying updraft used in this study is consistent with their value at the level where the updraft is a maximum. The effect of varying the amplitude is explored using a constant updraft which also gives information on how the shape of a vertical velocity profile would affect the distribution of precipitation.

(4) Other schemes that have been tested

A scheme was designed and computations made for precipitation particles with different fallspeeds but obeying the Marshall-Palmer distribution at all times. The results however, do not show appreciable differences from the single velocity case. The computations therefore, will not be presented here. Calculations are also made with the different drop size categories but including only collection of cloud in the accretion term. This scheme failed to develop a realistic drop-size distribution and therefore collection of precipitation by larger precipitation particles was included in further computations.

B. Results and discussion of results

(1) Relation of parameterization schemes to the distribution of cloud and precipitation and to surface rainfall rate

i) Microphysical parameterization

The first set of results (figures 6 to 9 and 16 to 19)

includes computations on the one-dimensional model where a Marshall-Palmer distribution in particle sizes and a single median drop terminal velocity are assumed. These are very similar to Kessler's original computations except with a type of circulation in which the cloud top rises instead of having motion initiated simultaneously throughout a deep layer.

Fig. 6 shows the distribution in cloud and precipitation water for two values of the autoconversion rate K, which governs the speed of generation of rain water from cloud droplets. A higher K is seen to increase the precipitation water content and correspondingly decrease the cloud amount. However, this effect is slight; for a sixfold increase in its magnitude form 0.001 sec^{-1} to 0.0062 sec^{-1} adds only 0.1 g kg^{-1} of rain water at any level.

The association of larger rain content with a bigger K value is reflected also in the surface precipitation patterns (see fig. 16). The stage of rapid development of the cell after 4200 seconds is marked by more intense rainfall for a faster rate of autoconversion. But the relation is not always valid. In fact, the opposite is shown in the precipitation curves at some earlier times. It should be noted that in the model, the increase in precipitation is the combined effect of the autoconversion and accretion processes. A faster autoconversion rate might deplete the cloud amount to such an extent that subsequent growth by accretion is hindered. Thus there exists a tendency for a balance to be reached and the resulting precipitation rate is not greatly

affected.

Three autoconversion thresholds namely a=0.5, a=1.0, and a=2 g kg^{-1}, are used for sensitivity analysis. The result in fig. 7 indicates the relative unimportance of varying the threshold value from 0.5 to 1.0. When a is set to 2 g kg^{-1}, the profile of precipitation becomes bell-shaped. The large amount of cloud present especially near the level of maximum updraft contributed tremendously to the build-up of rainwater at a later time.

It is interesting to find that a larger threshold can sometimes produce a heavier gush of rain (see fig. 17). This happens when the process of cloud accretion dominates over that of autoconversion. The precipitation curve corresponding to a threshold of 2 g kg^{-1} again shows a drastic departure from the other values.

The time of onset of precipitation at the surface is influenced greatly by the autoconversion threshold which determines when precipitation particles are generated. Fig. 17 shows that this time of onset increases with an increasing threshold. For the two lower values the time lag is about 300 seconds while a delay of more than 1000 seconds is required between the a=1 and a=2 g kg^{-1} cases.

The effect of a vertical variation of the threshold is explored using two linear functions; a(inc) and a(dec) described previously. The cloud and precipitation profiles for an increasing threshold is displayed in fig. 8 . They resemble those with a constant a of 0.5 and 1.0 g kg^{-1}. Some differences are seen at the surface rainfall. In the former case(fig. 18) rain at the ground begins

earlier as no threshold is imposed at the cloud base. Interesting features are revealed when the threshold decreases in the vertical. Precipitation particles originating at higher levels grow rapidly when they fall through the dense cloud layer near the base region. This brings about a rapid increase in rain water near the cloud base and a very strong pulse of precipitation at the surface (fig. 8 and fig. 18). Although the precise manner in which the autoconversion threshold may vary as a function of height is not known, the case with a decreasing threshold may simulate to some extent the effect of natural glaciation or of seeding a cloud where conversion of cloud to precipitation is accelerated at a high level.

The relative importance of precipitation growth by cloud accretion is studied by varying the collection efficiency. The results for E_c=0 and E_c=0.8 are shown in fig. 9 , the former corresponds to precipitation growth through only autoconversion. The distribution of cloud and rain water in that figure can be used to infer the role of cloud accretion. It is seen that at 3400 seconds, the precipitation water distribution for the two efficiencies are practically identical, indicating that at an early stage of rain formation, the autoconversion effect dominates over that of collection of cloud. The latter effect accelerates rapidly with the creation of more cloud water by condensation, and becomes equal in strength to the autoconversion process around 4400 seconds. The surface rainfall (see fig. 19)

reacts in a like manner. The precipitation rate with a zero efficiency is only about 40% of that with accretion included.

The same sensitivity tests are repeated with the division of precipitation water into nine size categories. The results shown in figures 10 to 15 for cloud and precipitation water and figures 16 to 19 for surface rainfall rate demonstrate similar effects in the variation of autoconversion parameters and cloud collection efficiency to those discussed above. For comparision, cloud and precipitation profiles in the case of a single fallspeed at 4800 seconds are also indicated.

These results reveal two major dissimilarities in the different modes of treating the precipitation water. In the first place, the case with nine size categories appears to have more precipitation at the upper levels. This phenomenon is the result of the piling up of precipitation water around the level of maximum vertical velocity where drops in the smaller categories are unable to fall against the strong updraft. Secondly, the surface rainfall curves (figures 16 to 19) point out that the multiple fall velocities case has a smaller precipitation rate at the earlier stages of cell development. As autoconversion creates only the smallest drops, the initial fallout of precipitation is expected to be slow until larger particles are developed. Indeed the formation of bigger drops at a later time rapidly increases the rainfall rate to surpass that of the single fall velocity case

in the long run.

A more lengthy computation for the evolution of the different size categories using Berry's autoconversion formula for maritime and continental clouds was performed. The updraft is turned off shortly after 4800 seconds when the cloud reaches its top level; however in this case continued rainout is allowed to take place until the termination of the computation at 7000 seconds. The maritime cloud contains more precipitation and also more cloud water than the continental one (fig.20,21). The latter produces more rain at the surface before the updraft was turned off.(fig 22) A characteristic splash down of precipitation is seen in both cases at 5100 seconds. This is caused by the rapid fallout of precipitation drops which now do not have to fall against the updraft.

A comparison of cloud and precipitation profiles (figures 20 and 21) using Berry's and Kessler's autoconversion formulae indicates a close resemblance of results. In fact Berry' continental case corresponds almost exactly to that of Kessler's with respective values of 0.001 sec^{-1} and 1g kg^{-1} for K and a, while the results with Berry's maritime formula differ very little from those using Kessler's expression with K=0.0062 sec^{-1} and a=0.5 g kg^{-1}. The implication then is that the exact form of the autoconversion equation is of little consequence in the evolution and distribution of precipitation. Furthermore, it indicates that Kessler's simple relation can be used to simulate different processes by an appropriate choice of constants.

It is not possible to make exact comparisons of the above results with sensitivity tests on microphysical parameters in other models, which are either dynamic in nature or possess a rather different circulation. However some similar conclusions on the effects of varying the autoconversion rate and threshold, or in changing the cloud collection efficiency, have been reached by Kessler (1969) and Weinstein (1969).

Kessler has shown the association of a general increase in the pulse of initial precipitation with a decreasing threshold and noted in particular the resulting heavy gush of rain when the autoconversion threshold is large in the lower altitudes and decreases with height. On the other hand, the magnitude of K was found to be rather unimportant after precipitation has become established but the height of a pulse-shaped transient near the start of precipitation is enhanced as the value of K decreases. For the cases with E_c=0 and E_c=1, he concluded that the steady state precipitation rate is lower in the latter case.

Weinstein has demonstrated the relative unimportance of the autoconversion rate. He varied its value over two orders of magnitude (from 10^{-2}sec^{-1} to 10^{-4}sec^{-1}) and found that in general a less than 10% differences in total rain amount, time of initiation of precipitation, maximum updraft velocity and height of cloud top are produced. The threshold, when varied over a range from 0 to 6 g kg^{-1}, was seen to produce significant changes in rainfall characteristics especially near the upper limit. In addition, the conversion and collection rates in his model appear to have about equal importance,

and it is only when each is made quite small that the ultimate rainfall characteristics change drastically.

(ii) Updraft shape and intensity

Constant updrafts with intensities of -0.22,-0.34, and -0.50 mb sec^{-1} are used to investigate the effect on the distribution of cloud and precipitation by virtue of variations in the shape and intensity of an updraft profile. Figures 23 , 24 and 25 show a characteristic distribution with a great accumulation of precipitation in the lower layers of the cloud caused by the inability of the rain drops with small terminal velocities to fall against the updraft column. Except for a difference in magnitude, the cloud and precipitation profiles for different updraft intensities are quite similar. If the vertical velocity has been turned off but the rainout computed a splash down resembling those indicated in figures 20 and 21 would be anticipated, but with considerably higher intensity. The distribution of rain water as examplified by the two rather extreme updraft shapes used in the present study points to the possibility of inferring updraft profiles from radar-observed precipitation distribution or to serve as a guide for interpolating in-between cases. Further discussion of the nature of such inferences however, must be deferred until the distribution of radar reflectivity and the effects of a sloping updraft are explored.

The surface rainfall rate for the case of a constant updraft and multiple fall velocities is illustrated in fig. 26 . The precipitation curve rises sharply and shows some kind of oscillation.

Comparison of these results with those for a single fall velocity is not possible, as in the latter case, the small precipitation amounts below the strong updraft result in a small computed median dropsize. The corresponding fall velocity therefore is not representative of the actual fallspeed of the precipitation particles falling out of the cloud base.

2) Relation of parameterization schemes to precipitation particle-size distributions

i) Microphysical parameterization

The general characteristics in the space and time evolution of the precipitation particle-size distributions are shown in figures 27 and 28. The Marshall-Palmer (MP) distribution and a distribution by Geotis (1963) on New England storms are included for comparison.

It is interesting to note that at the surface (1000 mb) the evolved size spectrum lies about midway between the MP and Geotis distribution. Progressing upward, one finds a greater concentration of precipitation water into the small drop-size categories while the departure from the MP distribution increases.

The change of size distribution of precipitation water in the vertical indicates the importance of accretion and coalescence processes in the modification of a size spectrum. As only one size of particles exists in the beginning, subsequent broadening of spectrum must be attributed to the modification during passage down the updraft column. This result is in agreement with the finding of Srivastava (1967). He simulated numerically the modification of raindrop size distribution by coalescence, beginning

with a narrow distribution consisting of two sizes only, which was modified considerably and tended toward an exponential distribution. On the other hand, he found that an initial exponential distribution of the MP type undergoes comparatively little change.

The time evolution of the distribution (fig.28) at the surface indicates the broadening of a narrow spectrum as well as a movement of the centroid towards the larger drops as time proceeds. For the varying updraft considered, the early stages of its development are marked by an abundance of small drops.

The dependence of the distribution on the autoconversion parameters is also investigated. Figures 29 and 30 indicates that the distribution is not affected by a tenfold variation of autoconversion rate. At the same time, the difference in the size spectrum for the two values of threshold 0.5 and 1.0 g kg^{-1} is also small (see fig.31). This confirms once again the relative insensitivity to K and to the value of a in the range from zero to one. Comparison for other autoconversion thresholds in the figure is not meaningful as a large difference in precipitation water content exists.

The size distribution using Berry's autoconversion formula is found in figures 32 and 33 . Just as in the case for the cloud and precipitation water profiles, the size distribution conforms closely to that obtained with Kessler's linear relation for the appropriate choice of K and a. It should be noted in these figures that the similarity between the Geotis and computed distribution developed at 4800 seconds is still maintained at

5100 and 5400 seconds, except with an increase in the very large drops.

ii) Updraft shape

A very different distribution at the ground is obtained with a constant updraft (fig. 34). The strong vertical velocity at the cloud base prevents drops in the smaller categories from reaching the surface; as a result a truncated distribution occurs. The vertical variation of distribution (see fig. 35) differs also from that for the varying updraft. Large drops are present up to 700 mb, while small drops begin to dominate above that level. The results in this case and those obtained with a varying updraft may be considered as extremes of what is likely to occur in nature.

iii) Computed distributions of radar reflectivity factor

Use of a single empirical Z-M or Z-R relation in interpreting radar measurements assumes invariance of the drop size distribution in space and time. Hence if a change in size spectrum occurs, calculation may either over or underestimate the precipitation water content of the storm. This effect is demonstrated in this model calculation.

Two Z-M relations are used for comparisons with the computations. The form used by Kessler gives $Z = 1.73 \times 10^4 M^{7/4}$ $[mm^6 m^{-3}]$ for an MP drop-size distribution while a relation of $Z = 3 \times 10^4 M^{1.6}$ $[mm^6 m^{-3}]$ is obtained from the average of two empirical distributions by Geotis as illustrated in fig. 36. (curve A)

The reflectivity factor calculated from the computed drop-size

distribution using a varying updraft and Berry's autoconversion formula is plotted against the precipitation water content in figures 37 and 39 showing the variation of Z as a function of both time and space before the updraft is turned off, also plotted are the MP and Geotis relations. It is seen that in both the continental (fig. 37) and maritime (fig.39) cases, the MP and Geotis formulae which are based only on drop-size measurements at the ground underestimate the liquid water content for a given Z during the earlier stage of development of the cell. The same can also be said about the precipitation water content in the upward direction where both relations give a smaller precipitation at high levels.

Figure 38 and 40 depict the event after the updraft is suddenly turned off. A fairly straight Z-M curve is obtained. The fast accumulation of larger drops in the lower part of the cloud and below leads to a high computed Z value. In such a situation, the MP and Geotis relations will overestimate the precipitation water content for a given reflectivity factor. This is shown to be valid up to 700 mb.

The overestimation is also found in the constant updraft case. The truncated spectrum consisting of large drops near and below the base region results in a high Z value. The illustration shown in figure 41 indicates that the Geotis relation overestimates the water content at all times below 800 mb, while the MP curve gives a higher estimate at even a higher level.

The actual case in the atmosphere is anticipated to lie

between these two extreme updraft profiles. Nevertheless, the computations illustrate the importance of the shape and intensity of the updraft column in affecting the evolution and distribution of precipitation and calls for careful attention to the time and space evolution of drop-size distribution in the radar measurement of precipitation.

3) Limitations of the model

It is recognized that the varying updraft used in this study is unrealistic in giving a very slow start at the base. This does not only have the undesirable effect of wasting a lot of computation but also introduces small drops below the cloud at an early time and makes the entire cell-duration larger than seems to occur in nature. Future computations should aim at improving this situation by the use of a similar curve but with somewhat larger updraft speed near the base.

The finite difference scheme used introduces diffusion of cloud and precipitation. Although it is believed that this effect is small, it should be analysed carefully to determine its influence. In addition, the cloud base condition have to be improved. In actual situations, the cloud amount at the base is changed only by the accretion process, since in each successive wafers or parcel the same amount of moisture is condensed as it rises through any given layer.

Some microphysical aspects like water drop break-up, condensation on raindrops, and evaporation below the cloud base have not been included. However these appear to have only secondary effects.

Because the one-dimensional model is unrealistic in its configuration it seems unfruitful to explore them with it until the significant differences between the results with one and several dimensions are examined.

VI. SUMMARY AND RECOMMENDATIONS FOR FURTHER RESEARCH

A. Summary

This study is concerned with the development of techniques which serve as a diagnostic tool for parameterization schemes and to provide insight into understanding the relation among air motion, microphysics, and the distribution of precipitation. Due to the three-dimensional structure of atmospheric motions, a three-dimensional model is needed for adequate consideration of relations between air motion and distribution of hydrometeors. The work is carried out in two major steps. The first part involves the formulation of a three-dimensional kinematic model based on a set of continuity equations with specified kinematics and microphysics. Second, the effects and importance of the roles of the microphysics and the updraft forms are tested with the one-dimensional model.

The sensitivity of the distribution of cloud and precipitation water to the formula for autoconversion of cloud to rain was tested by computing distributions with Kessler's linear formula using several values of autoconversion rate and threshold. Comparison of these results with each other and with those obtained with formula derived by Berry (1967,1968a.1968b) which is based on a more detailed calculation of the physical processes shows that the actual form of the assumed autoconversion function is relatively unimportant. The autoconversion rate K in Kessler's linear relation

is found to contribute very little to the change of precipitation patterns. The autoconversion threshold α exhibits little effect in the range of values from 0.5 to 1.0 g kg^{-1}. An increase beyond this range, however, is seen to produce large changes in cloud and precipitation. From this finding it is concluded that the simple linear parameterization is justifiable provided the constants are chosen so that the rate of conversion is compatible with observed lifetime of cumulonimbi and available computations of the physical processes.

The division of precipitation into different size and fall-speed categories as compared with the assumption of an exponential size distribution and one fall velocity is shown to be important in the formation and evolution of precipitation. The model computations indicate a narrowing of the drop-size spectrum upward into the cell and reveals the feasibility of developing an exponential spectrum from initial narrow distribution by the accretion and coalescence processes.

The updraft shape and magnitude, especially near the cloud base, influence strongly the distribution of precipitation and subsequent evolution of the size spectrum. With a stronger updraft speed near cloud base there is a considerably greater accumulation of precipitation in the lower portion of the cloud. The characteristic cloud and precipitation profiles displayed by different updrafts point to the possibility of inferring the shape and magnitude of the updraft column from radar-observed precipitation patterns.

This study demonstrates some of the difficulties in radar measurement of precipitation. Depending on the time and space evolution of the drop-size spectrum, interpretation of measured reflectivity in terms of liquid water content based on Z-M relations obtained from drop-size distribution measurements at the surface might significantly overestimate or underestimate the actual mass of precipitation present.

B. Recommendation for further research

Radar observations of precipitation distribution with high resolution both in time and space are recommended. This is necessary as existing radar measurements lack the resolution to provide a check on the results reported here.

The one-dimensional computation presented are preliminary studies needed for the purpose of using the three-dimensional model as a diagnostic tool. Therefore a logical extension is to include the two and particularly three-dimensional cases. The outcome of this study has provided a basis for a better model. It has been shown that the slow motion near the cloud base is unrealistic, both in the time of surface precipitation onset and in giving too many small drops at an early stage of cell development. Based on the findings of this thesis therefore, recommendation is made for the use of an intermediate updraft profile, a simple linear autoconversion function, and division of precipitation into nine size categories for the two and three-dimensional

computations. A two-dimensional model will be used to explore horizontal gradients in cloud water, precipitation and reflectivity and to compare the mean values at different levels with those obtained in one-dimensional case. The three-dimensional computation is necessary to explore the effects of wind shear, sloping updraft and motion of source and is the important one for comparing with radar data and interpreting them.

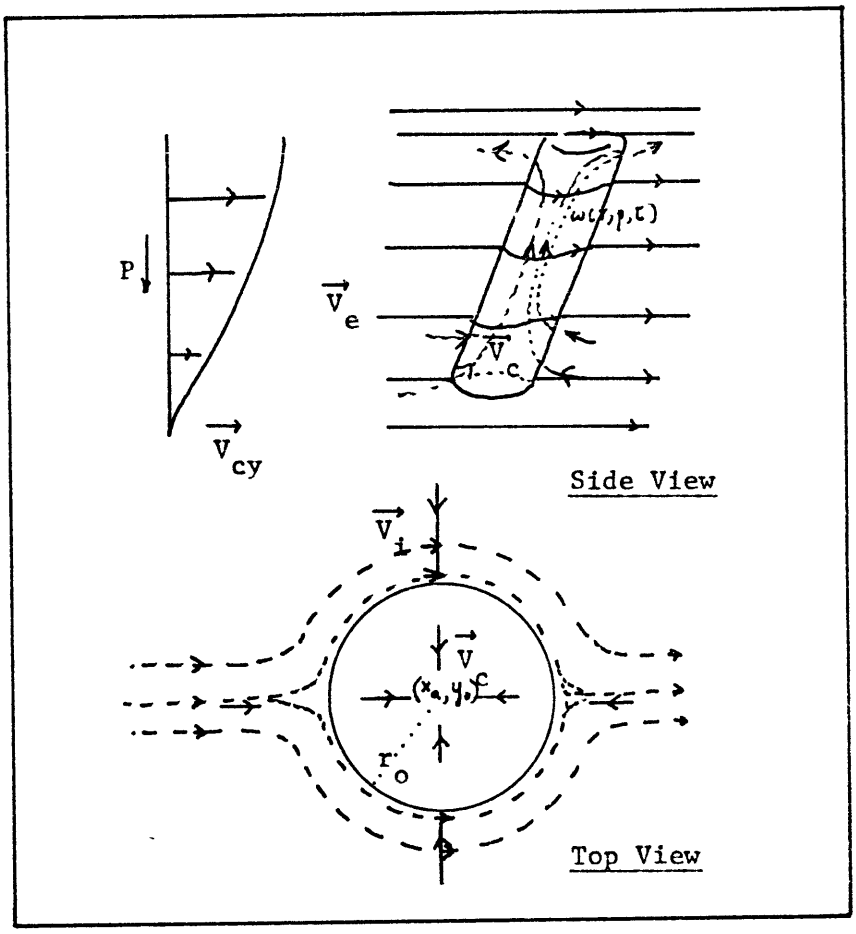

Fig. 1. Illustration of air motion in and around a model updraft.

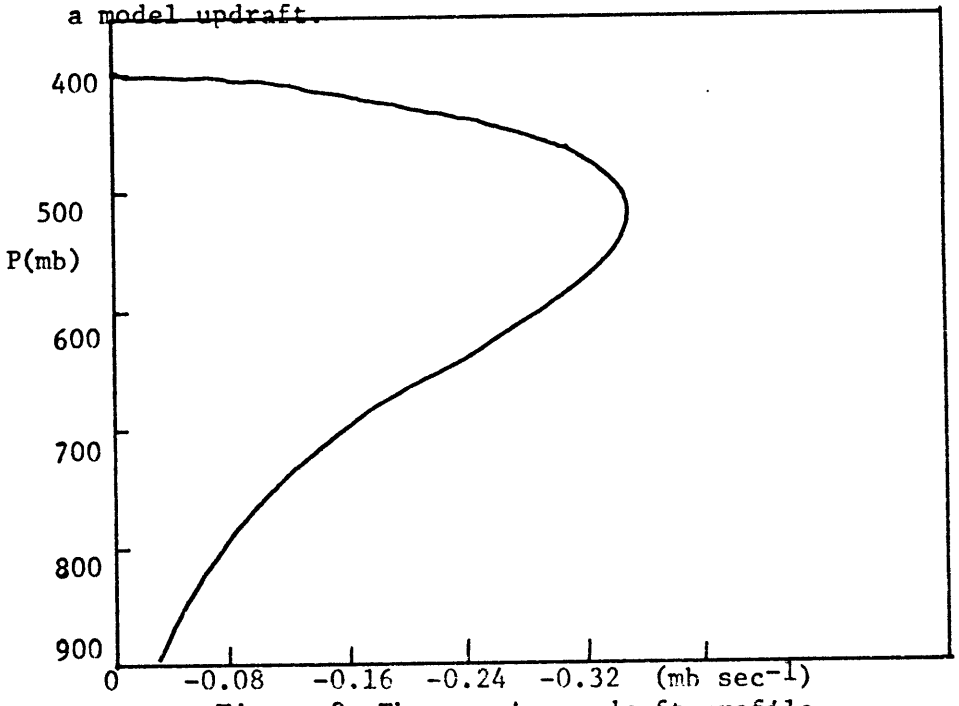

Figure 2. The varying updraft profile.

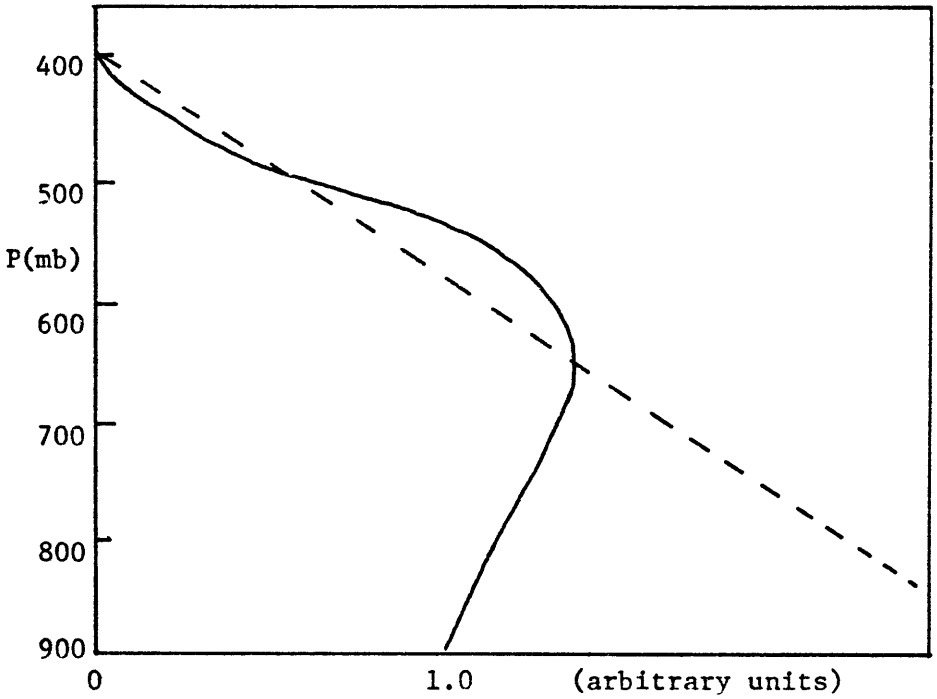

Figure 3. The shape of the mass transport curve.

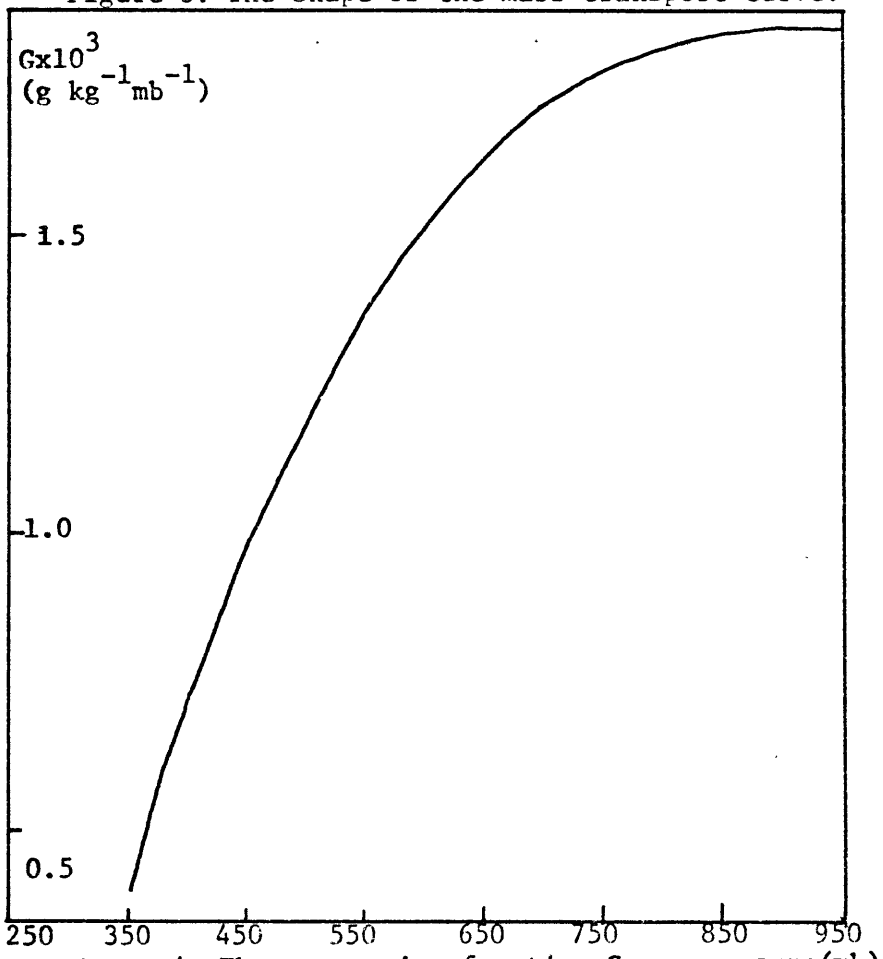

Figure 4. The generating function G vs pressure(mb)

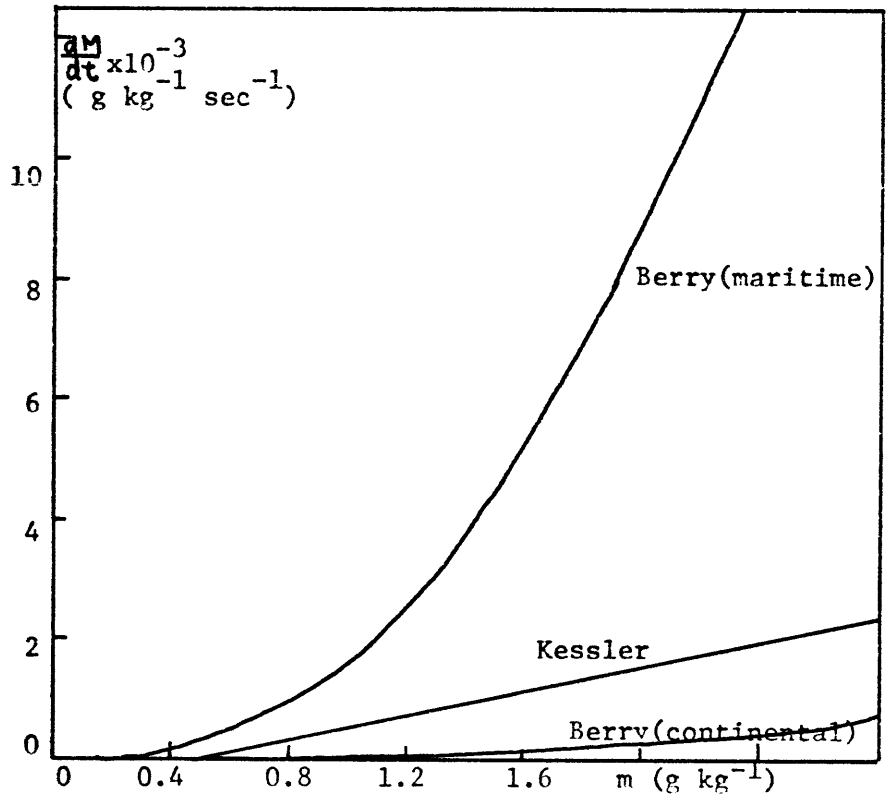

Figure 5. Comparison of Kessler's linear AC function (K=0.001 sec^{-1},a=0.5 g kg^{-1}) with Berry's AC formula for continental and maritime cloud.

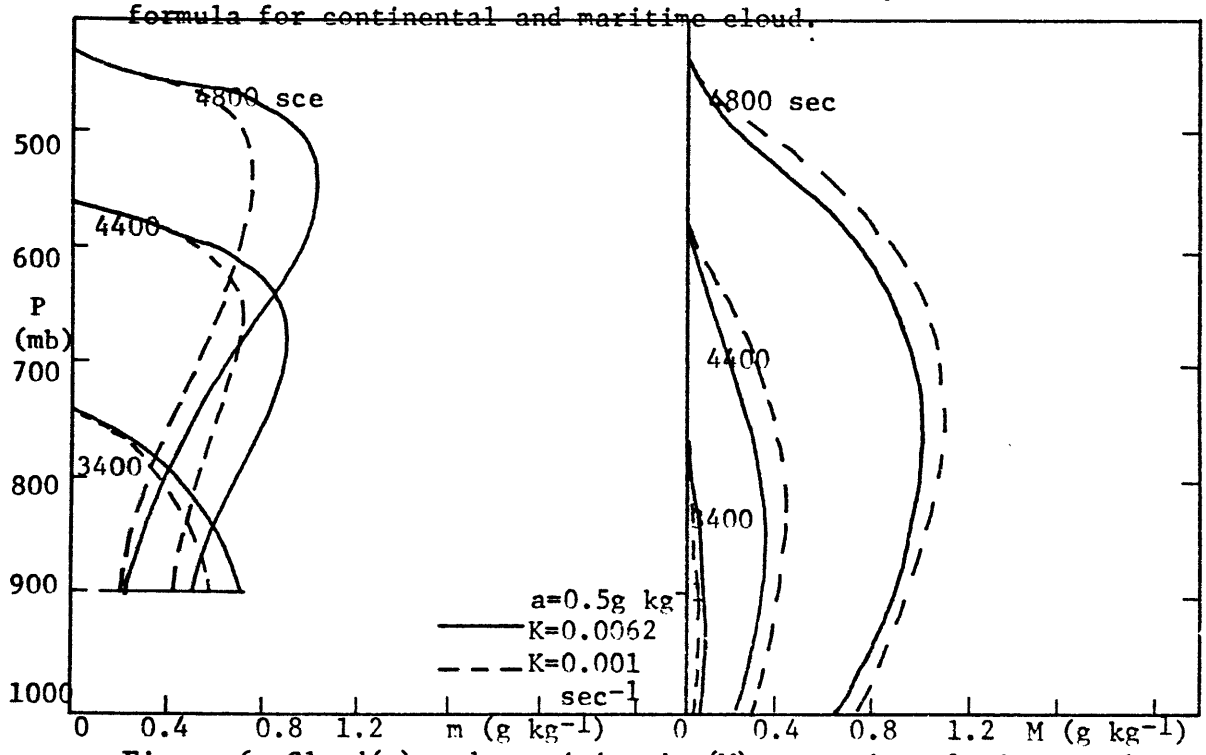

Figure 6. Cloud(m) and precipitation(M) water in relation to the autoconversion rate K-case of a varying updraft and single fall velocity.

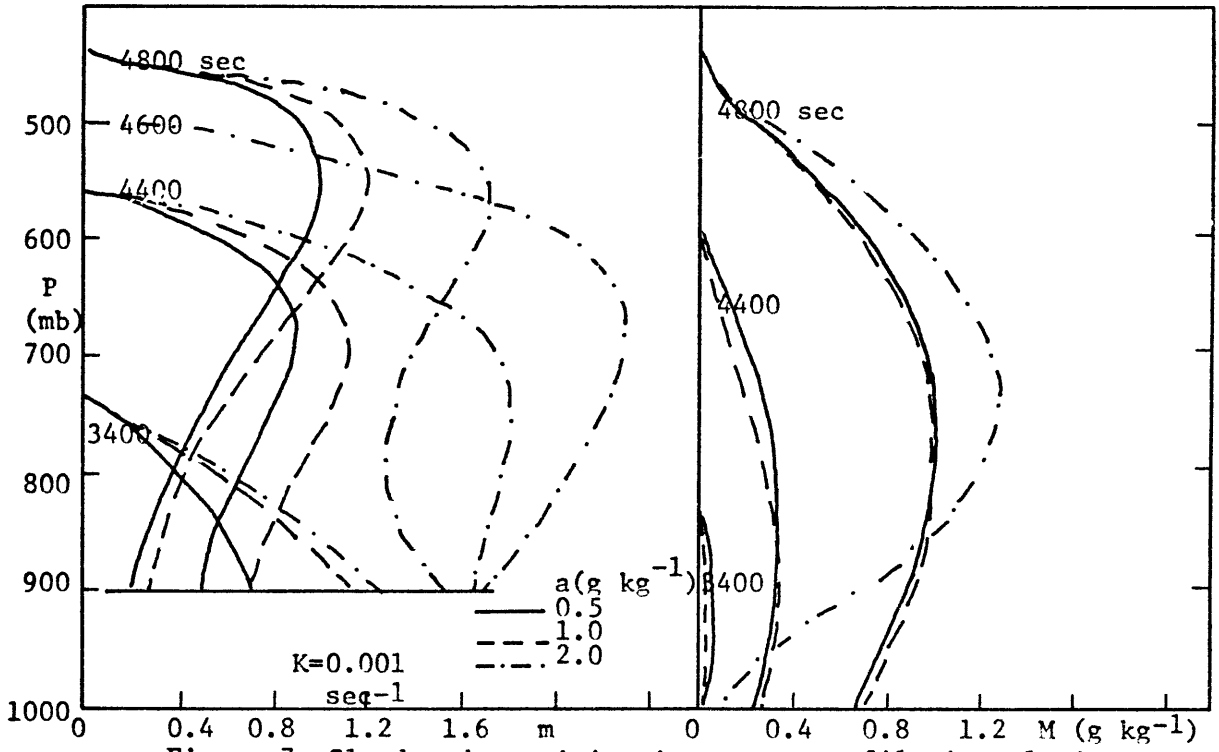

Figure 7. Cloud and precipitation water profile in relation to the autoconversion threshold a--case of a varying updraft and single fall velocity.

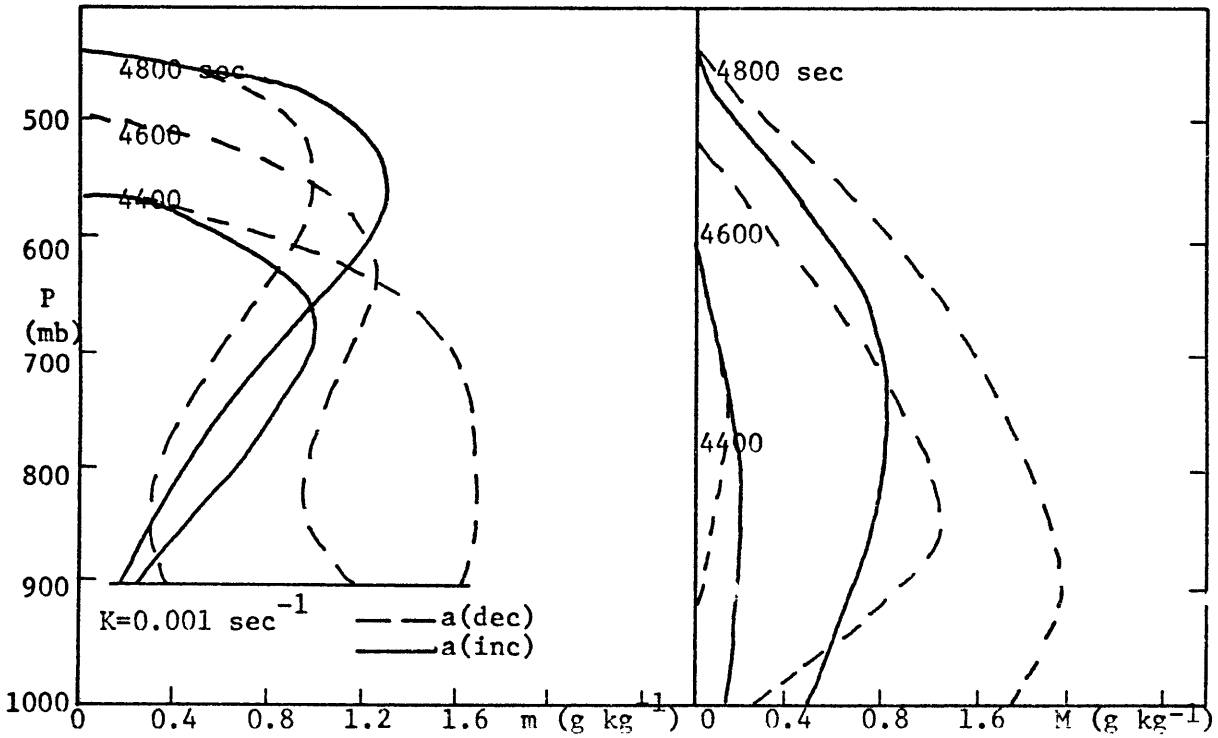

Figure 8. Cloud(m) and precipitation(M) water profile in relation to a vertical variation of the autoconversion threshold a--case of a varying updraft and single fall velocity.

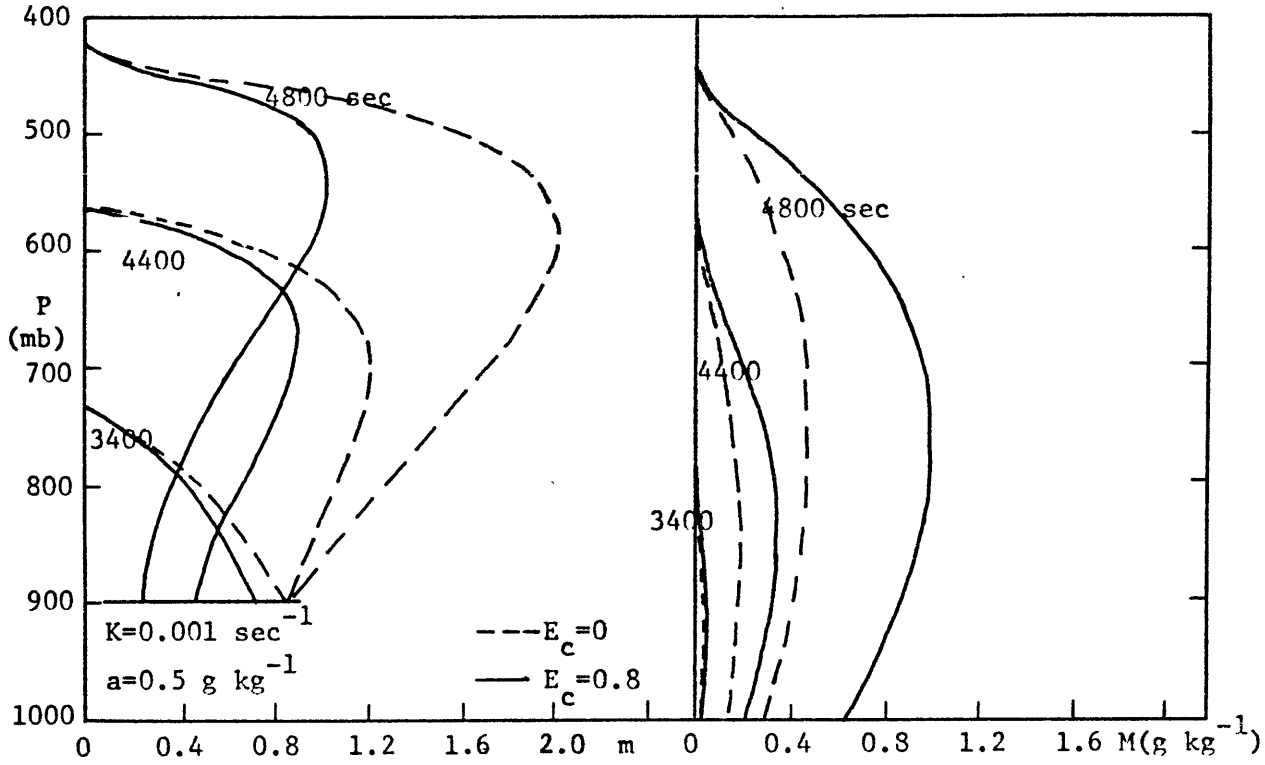

Fig.9 Cloud and precipitation water profiles in relation to the cloud collection efficiency E_c in the case of a varying updraft and single fall velocity.

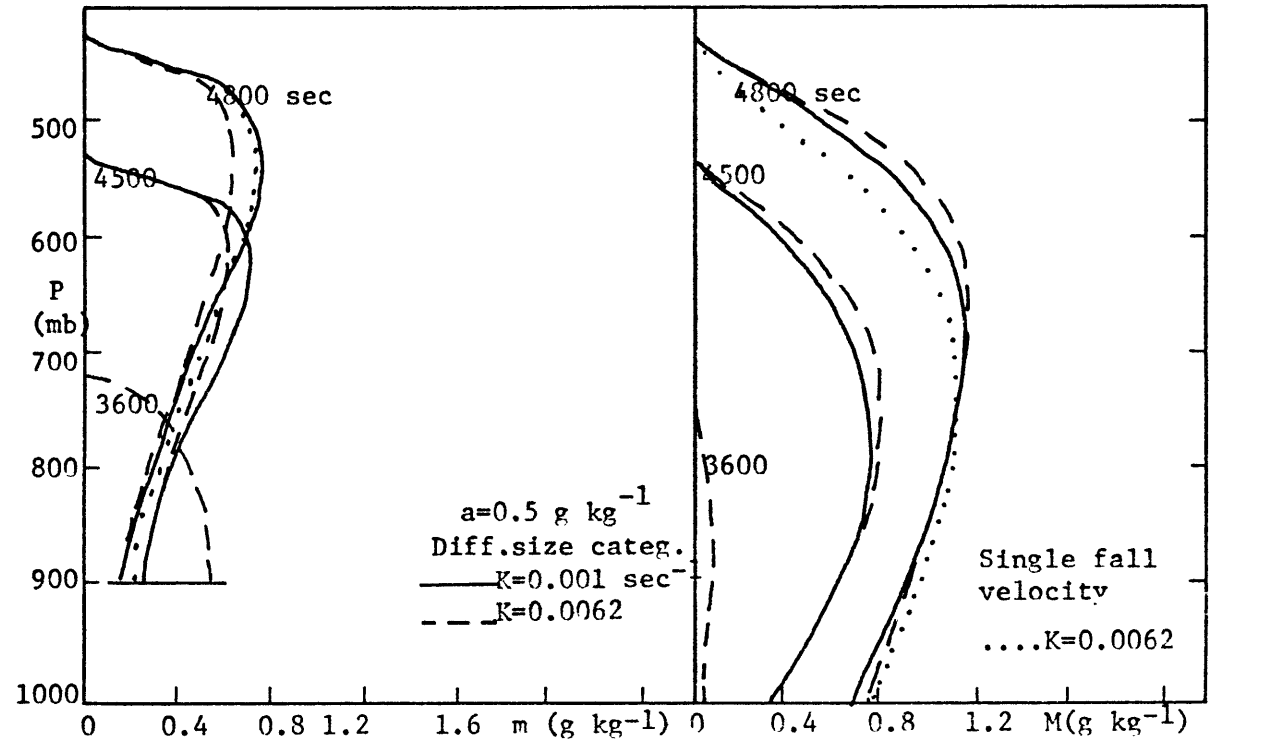

Figure 10. Cloud(m) and precipitation(M) profiles with different size categories in relation to the autoconversion rate K and comparison with those with a single fall velocity in a varying updraft.

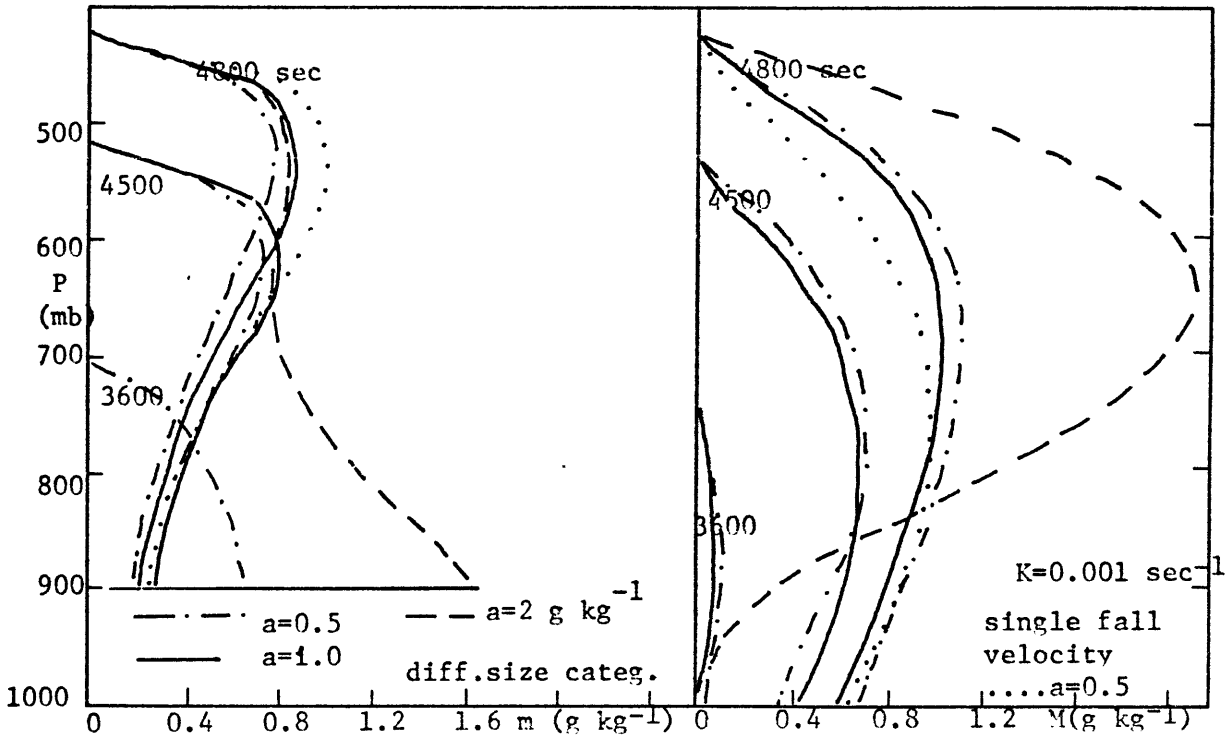

Figure 11. Cloud(m) and precipitation(M) profiles with different size categories in relation to the autoconversion threshold a, and comparison with those having a single fall velocity in a varying updraft.

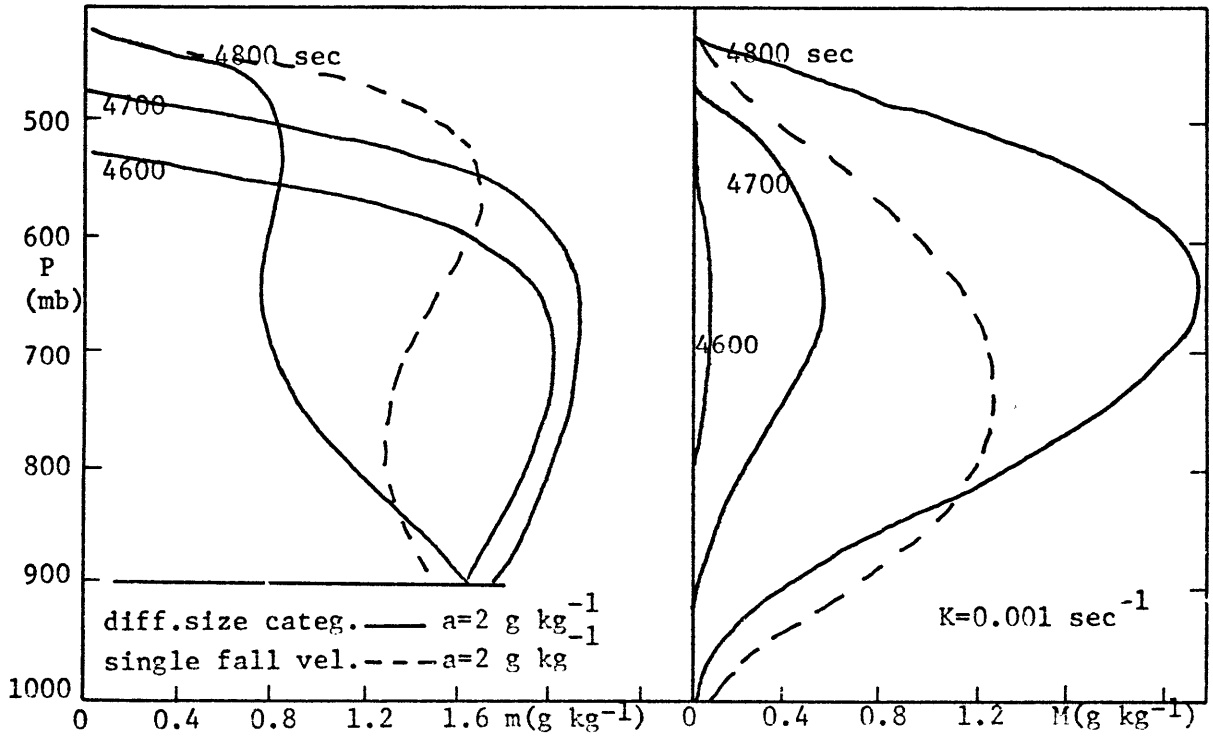

Fig. 12. Comparison of cloud and precipitation profiles with $a=2$ g kg^{-1} between the case with different size categories and those assuming a single fall velocity in a varying updraft.

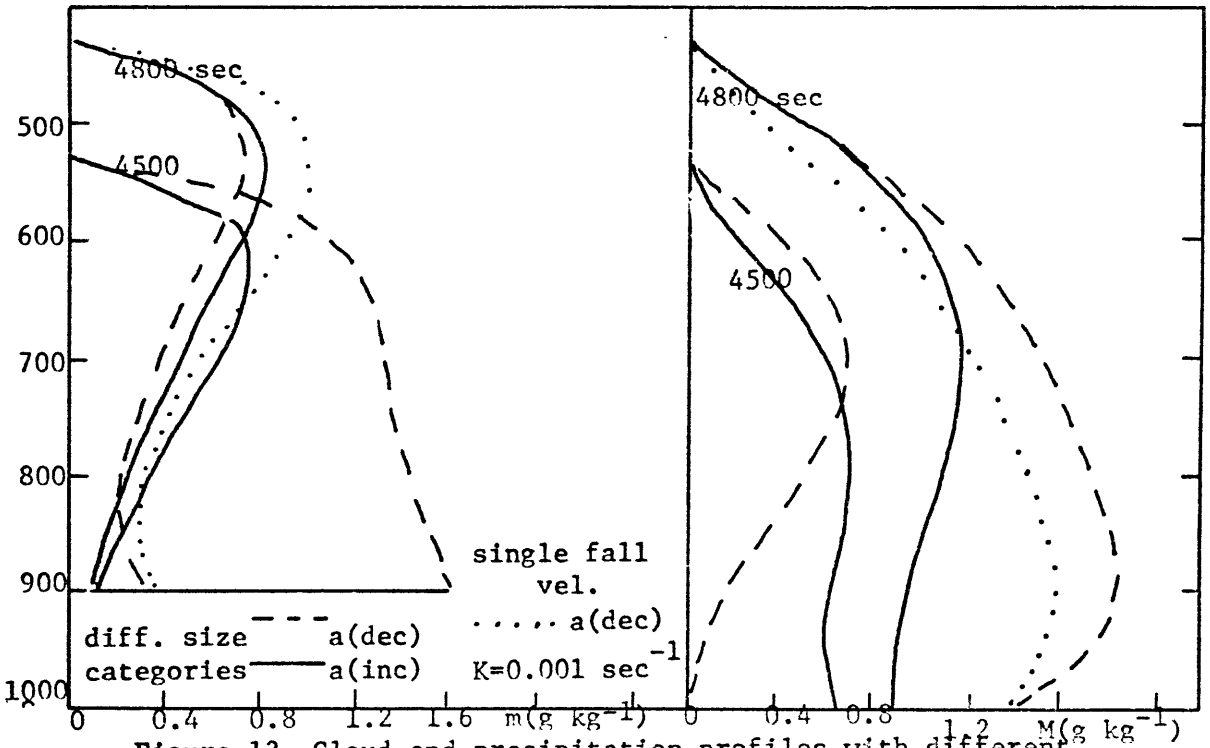

Figure 13. Cloud and precipitation profiles with different size categories in relation to the vertical variation of the autoconversion threshold and comparison with the case of a(dec) having a single fall velocity in a varying updraft.

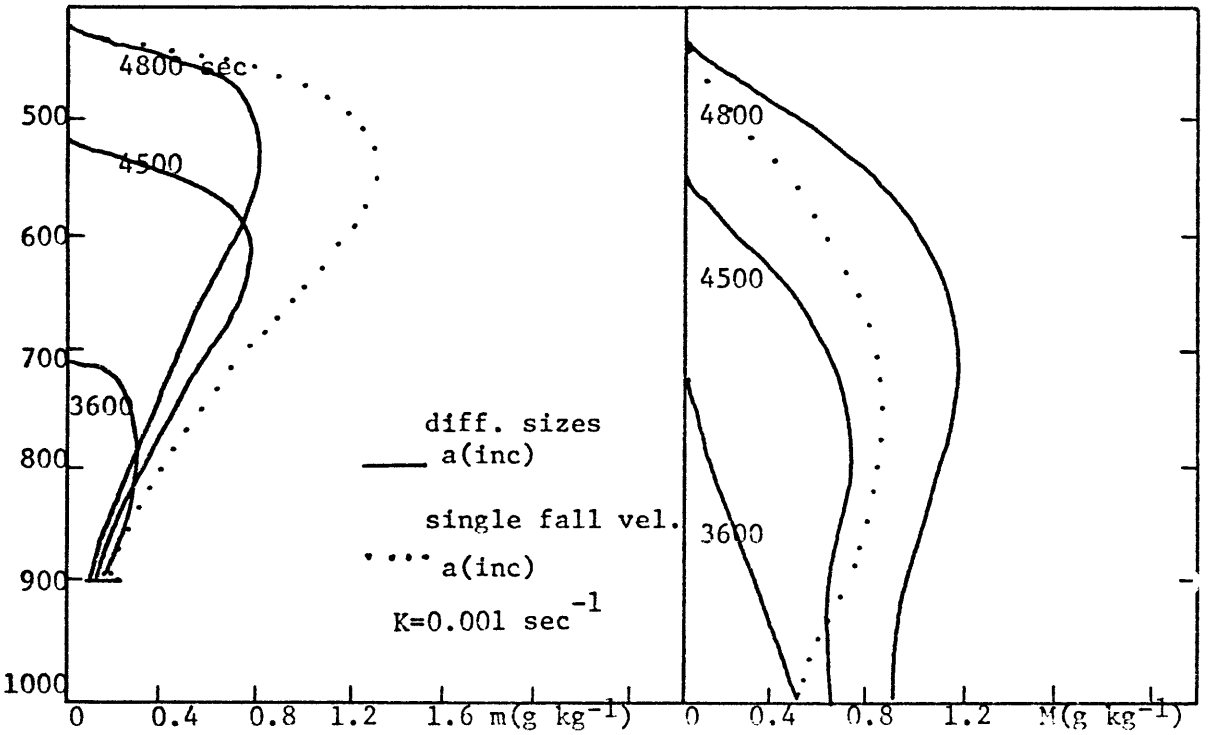

Figure 14. Comparison of cloud and precipitation profiles with a vertically increasing threshold between the case with different size categories and those assuming a single fall velocity in a varying updraft.

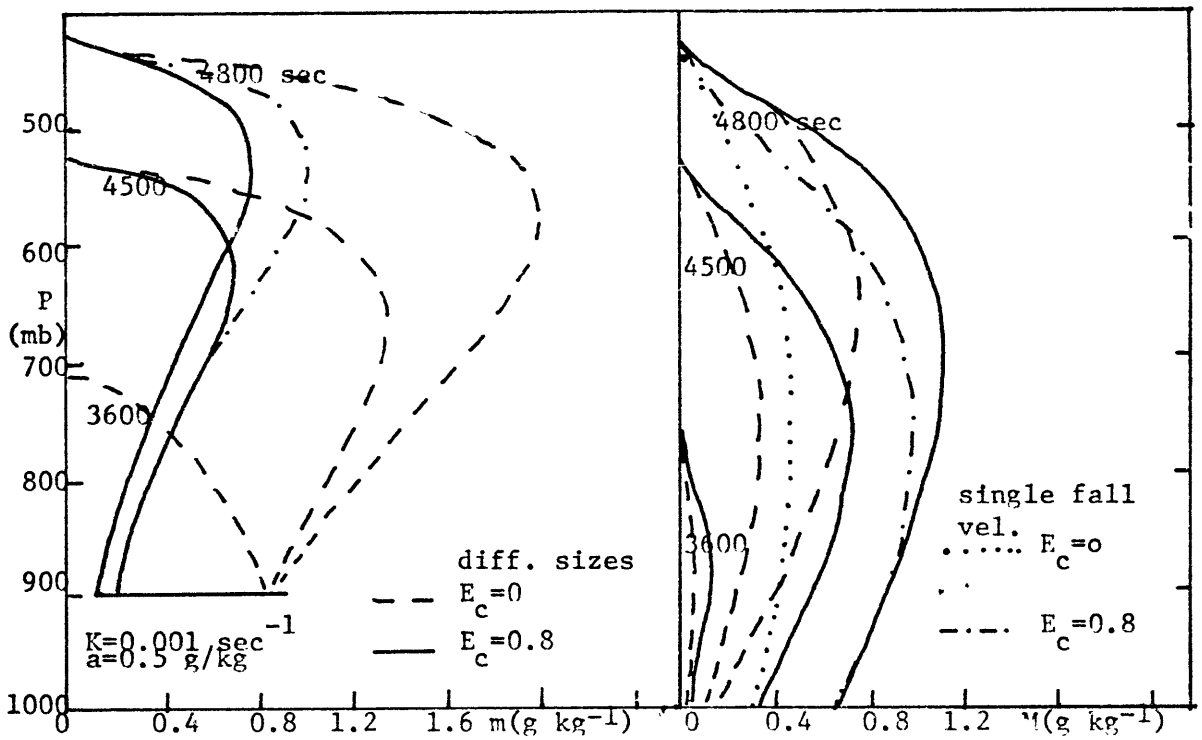

Figure 15. Comparison of cloud and precipitation profiles in relation to the cloud collection efficiency E_c between the case with different size categories and those assuming a single fall velocity in a varying updraft.

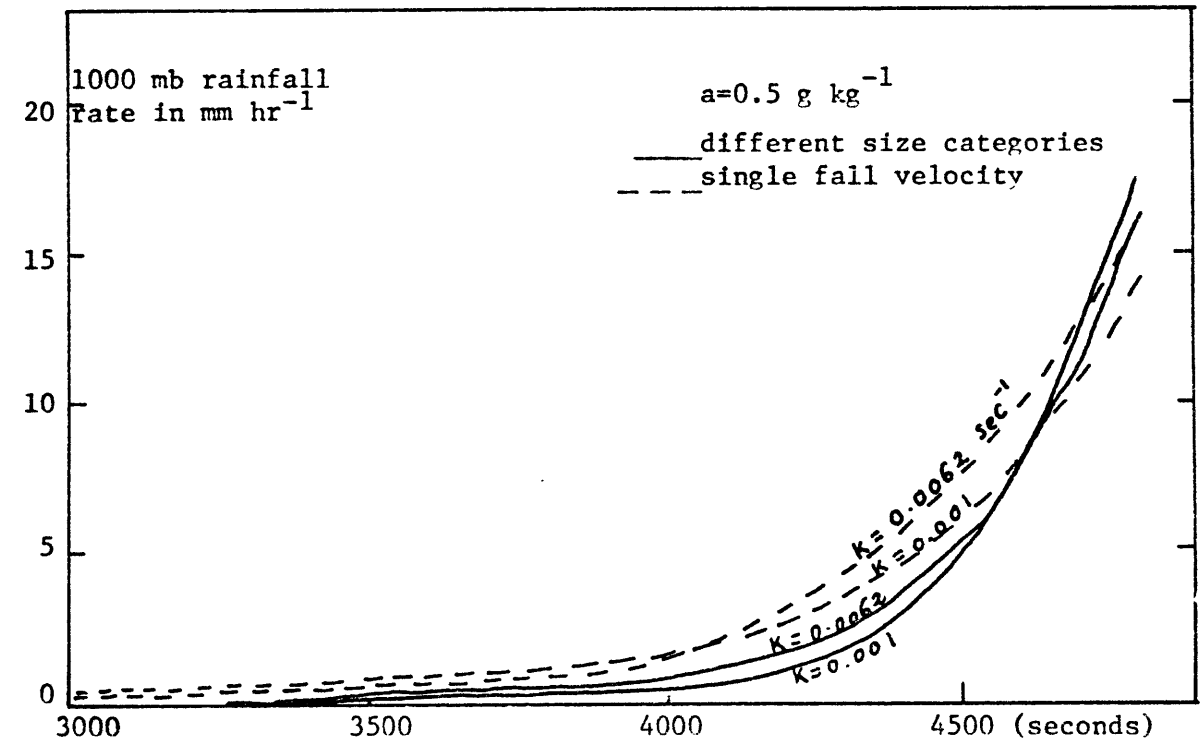

Figure 16. Surface rainfall rate in relation to the autoconversion rate K.

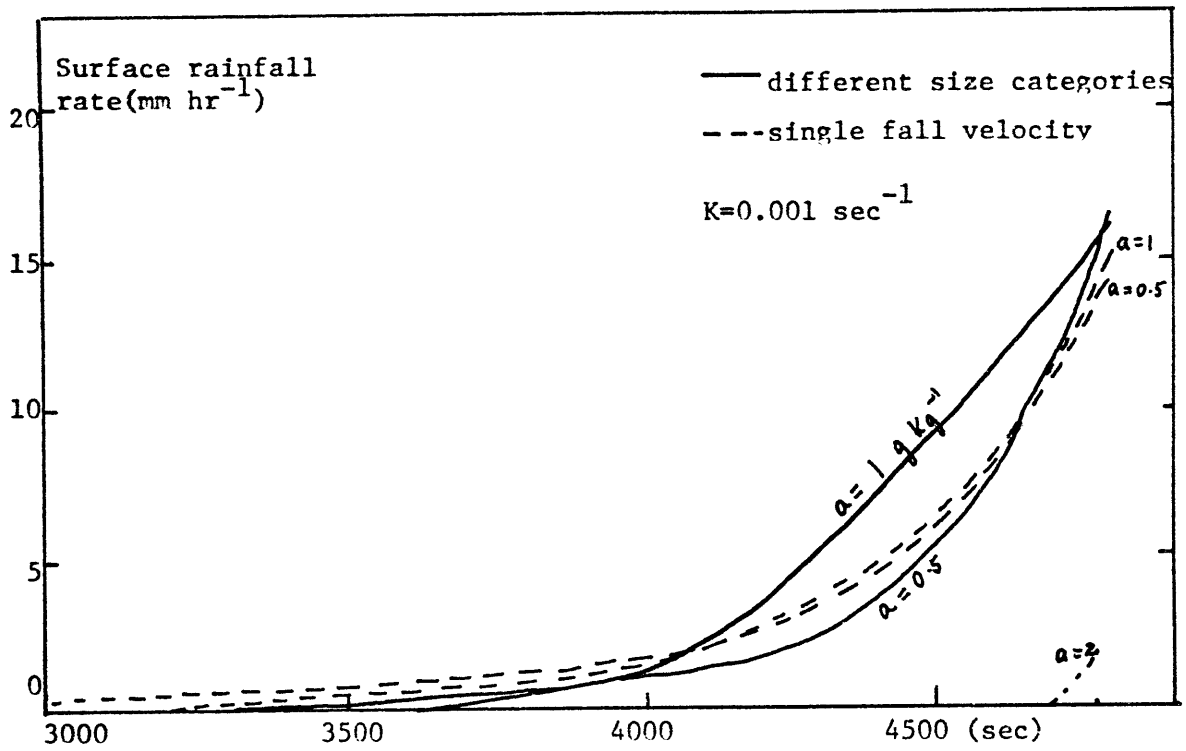

Figure 17. Surface fainfall rate in relation to the autoconversion threshold a.

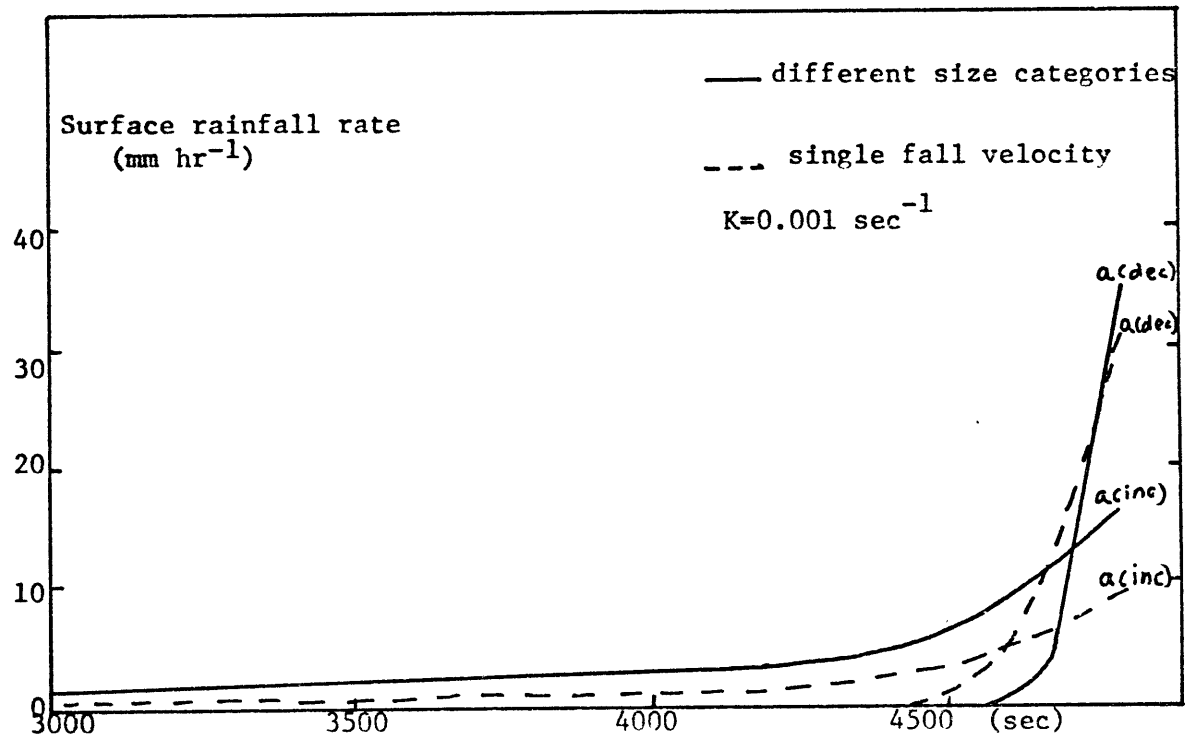

Figure 18. Surface rainfall rate in relation to the vertical variation of the autoconversion threshold a.

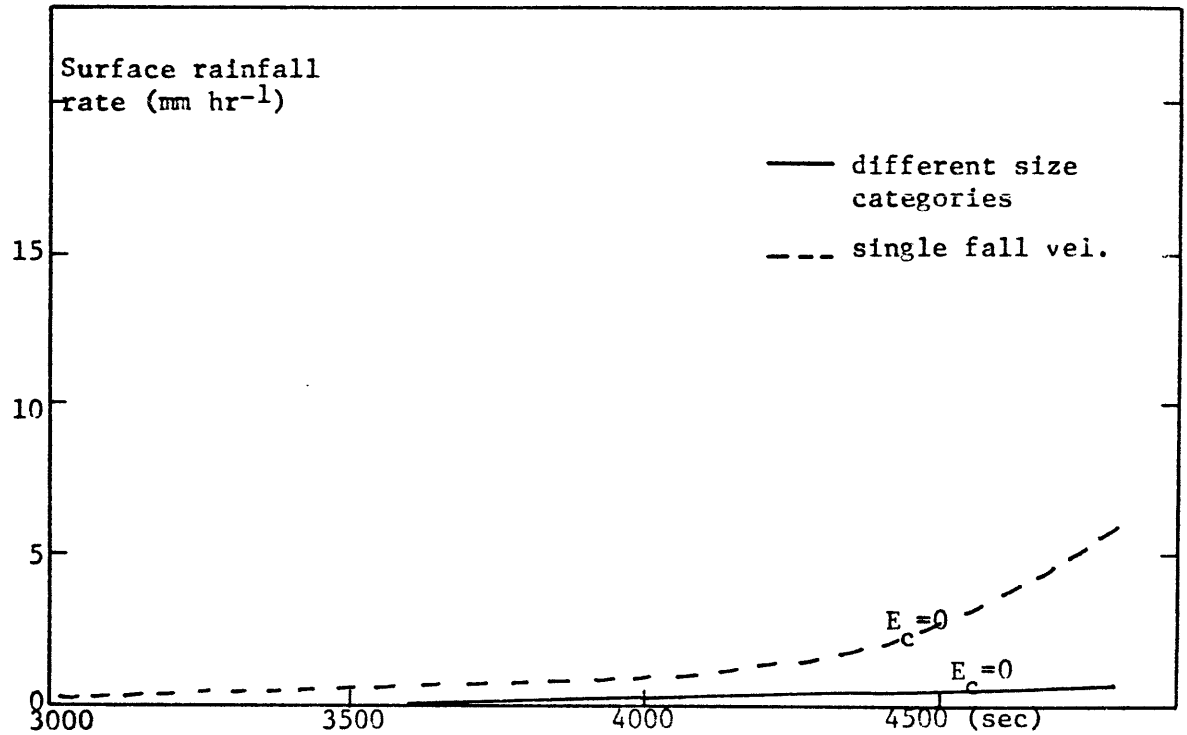

Figure 19. Surface rainfall rate in relation to the cloud collection efficiency E_c.

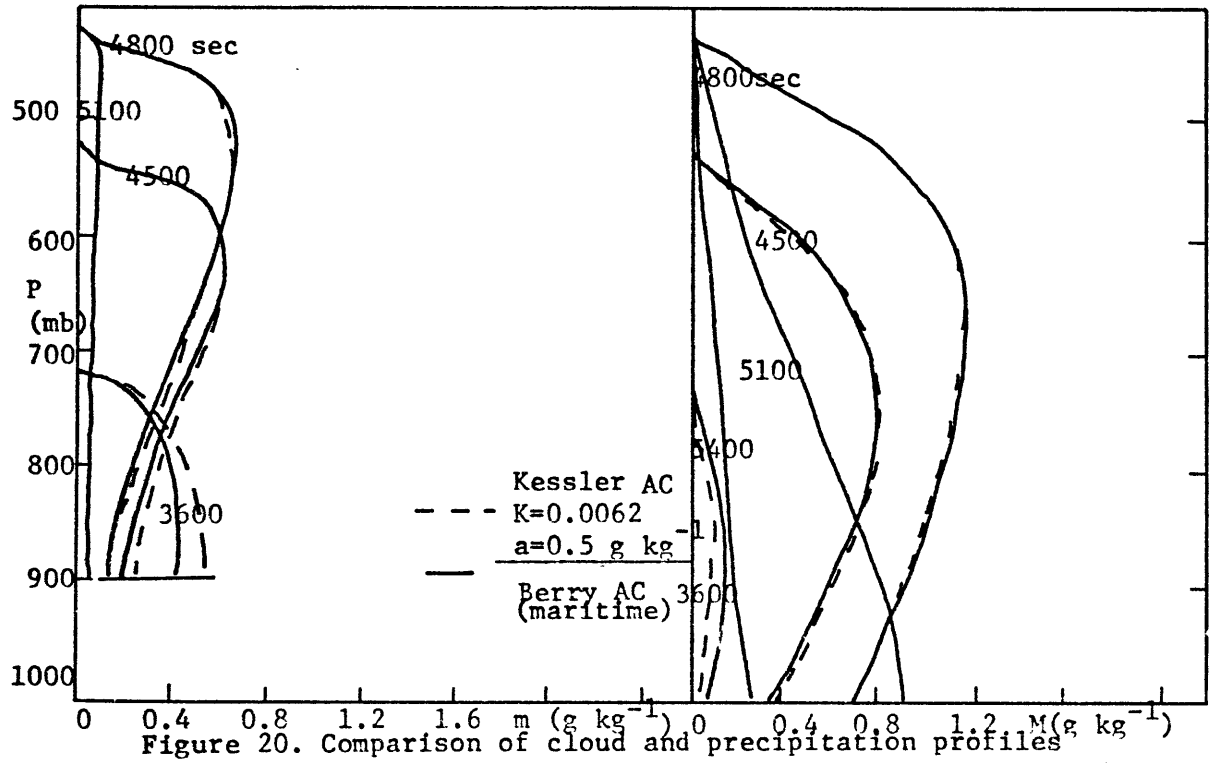

Figure 20. Comparison of cloud and precipitation profiles between Kessler's linear relation and Berry AC for maritime cloud.

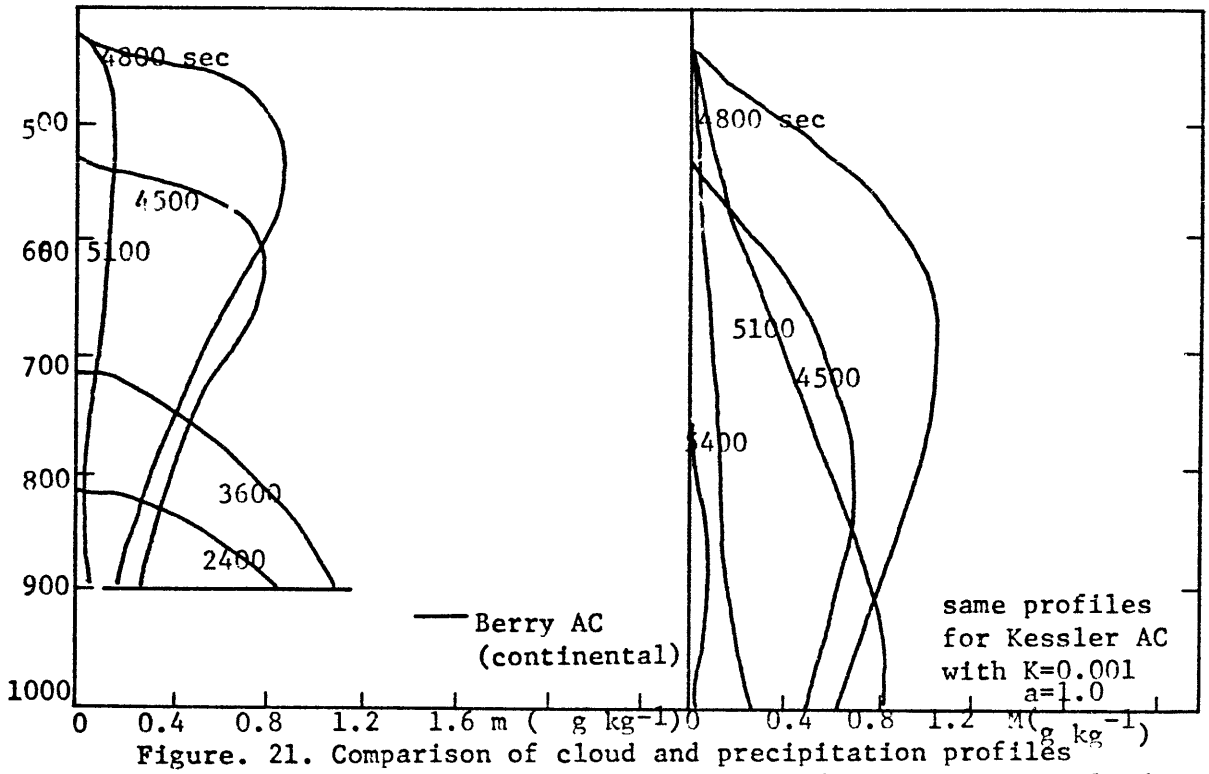

Figure. 21. Comparison of cloud and precipitation profiles between Kessler's linear relation and Berry AC for continental cloud.

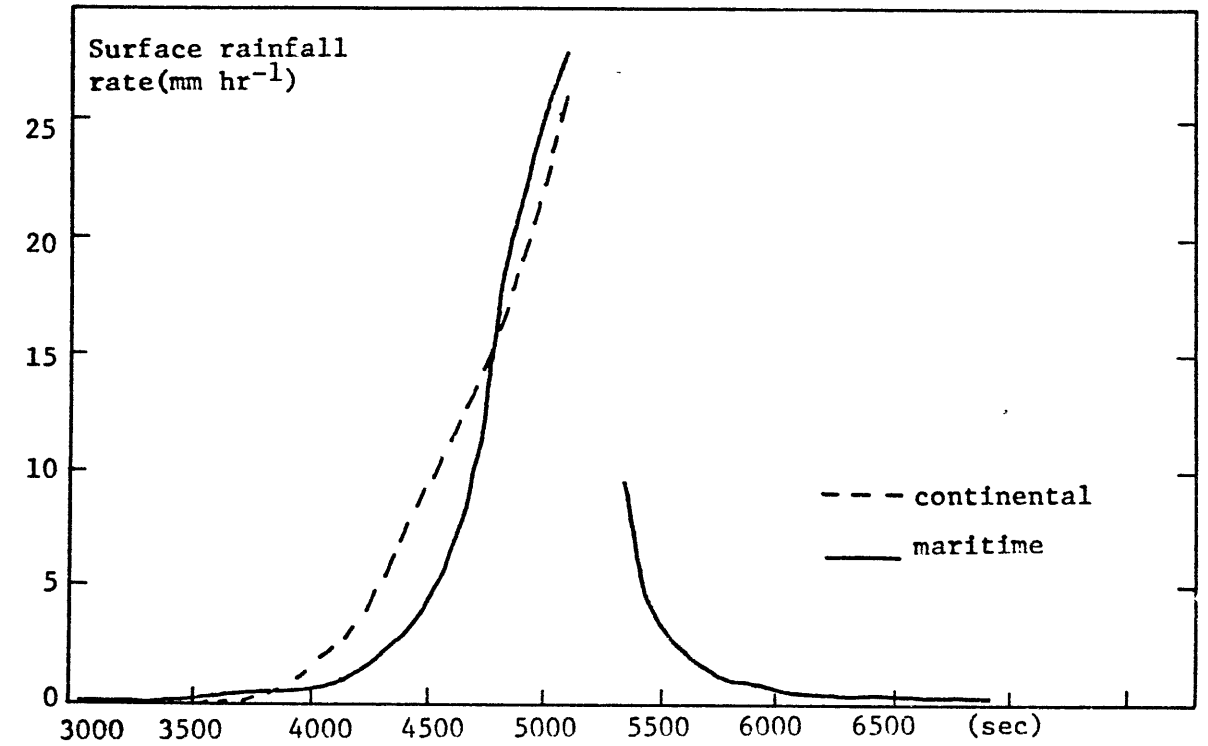

Figure 22. Comparison of surface rainfall rate using Berry AC for continental and maritime cloud.

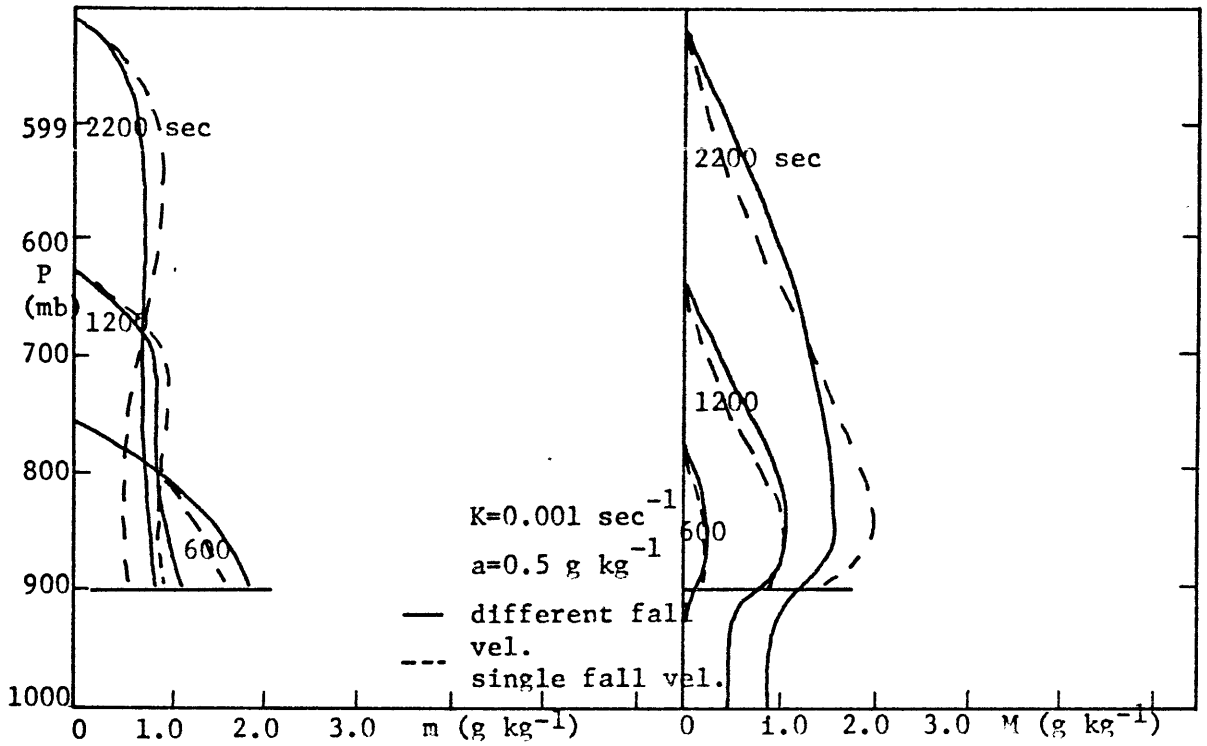

Figure 23. Comparison of cloud and precipitation profiles in a constant updraft of -0.22 mb sec^{-1} between the case of different size categories and that assuming a single fall velocity.

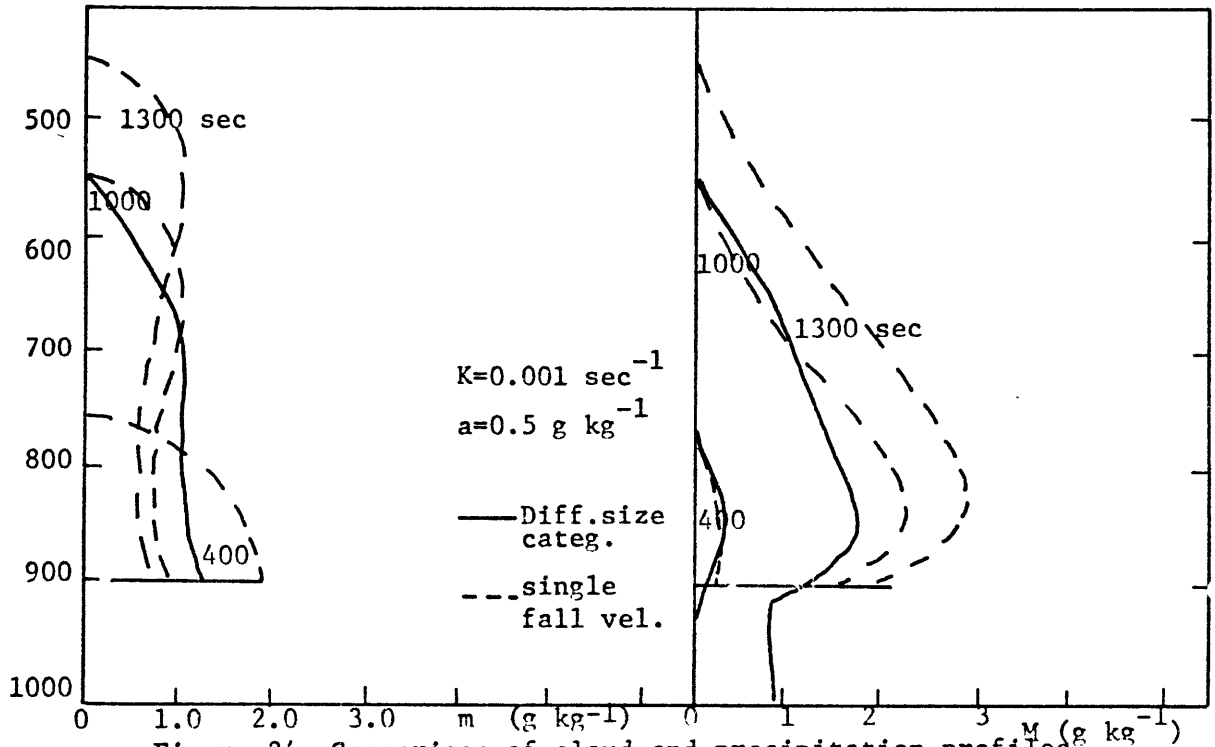

Figure 24. Comparison of cloud and precipitation profiles in a constant updraft of -0.34 mb sec^{-1} between the case of different size categories and that assuming a single fall velocity.

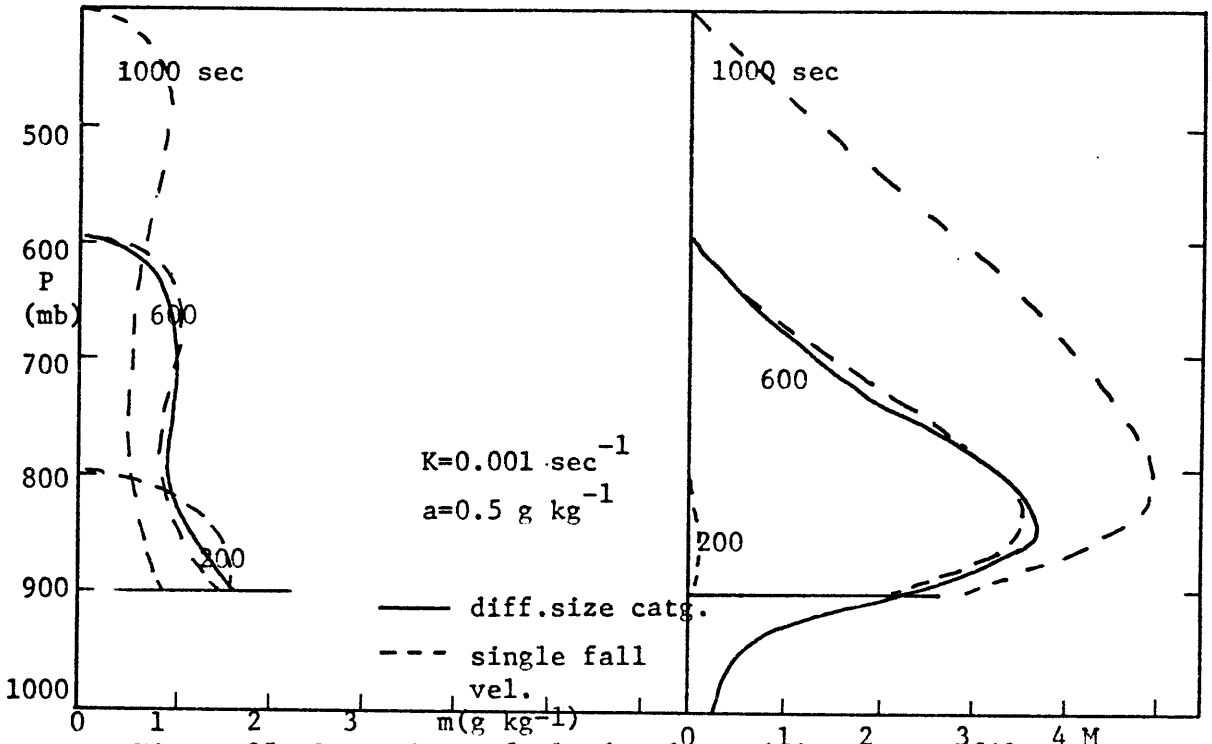

Figure 25. Comparison of cloud and precipitation profiles in a constant updraft of -0.5 mb sec^{-1} between the case of different size categories and that assuming a single fall velocity.

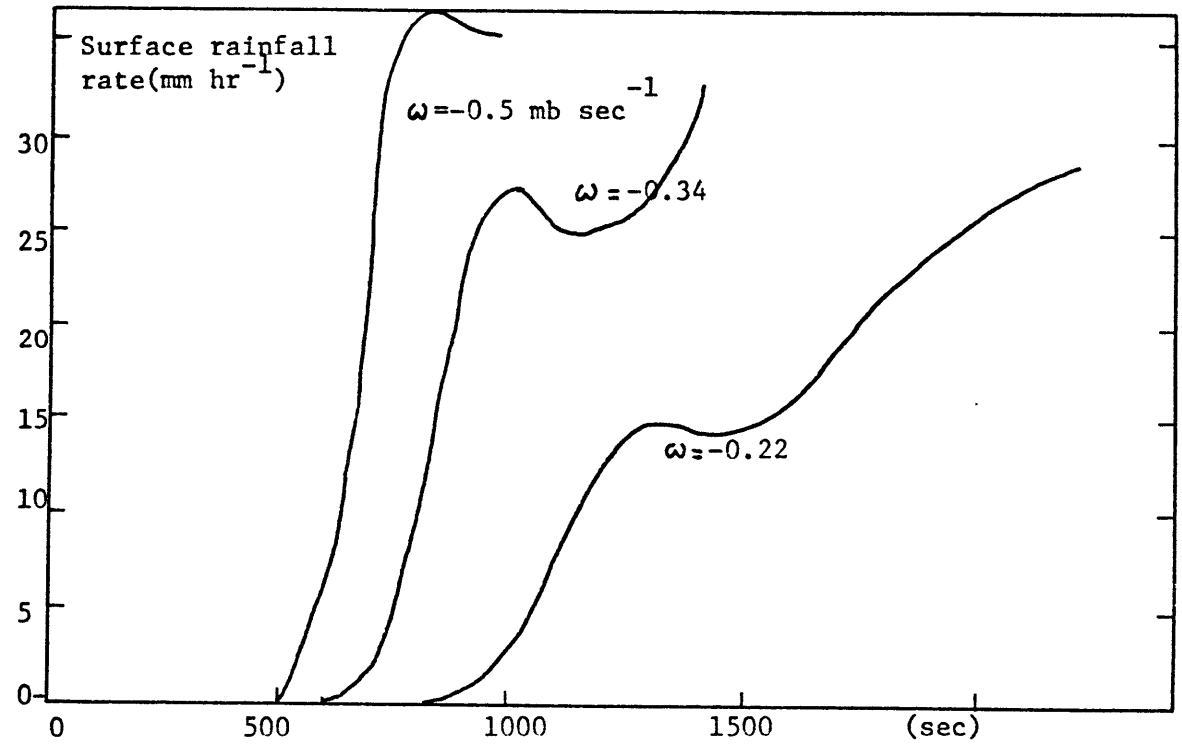

Figure 26. Effect of varying the intensity of a constant updraft on the surface rainfall rate using different size categories.

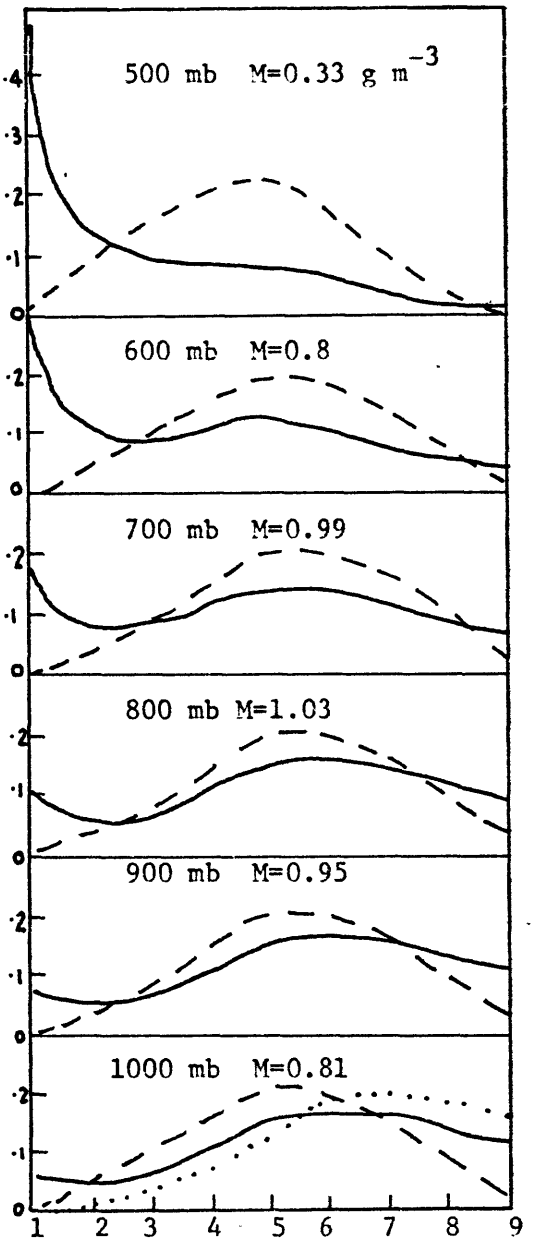

Fig. 27. The vertical variation of size distribution in a varying updraft at 4800 sec. Kessler AC used with K=0.001 sec^{-1} and a=0.5 g kg^{-1}. The vertical axis indicates the fraction of precip. water in each size category.MP and Geotis distri. included for comparison.

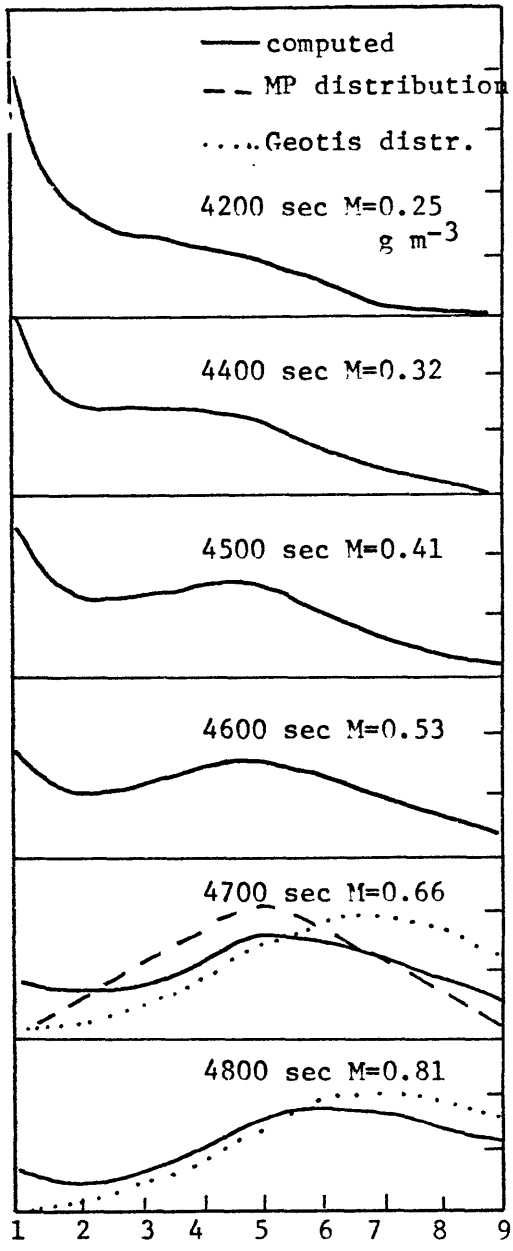

Fig. 28. Time evolution of size distribution in a varying updraft at 1000 mb. Kessler AC used with same values for K and a as in Fig. 27.

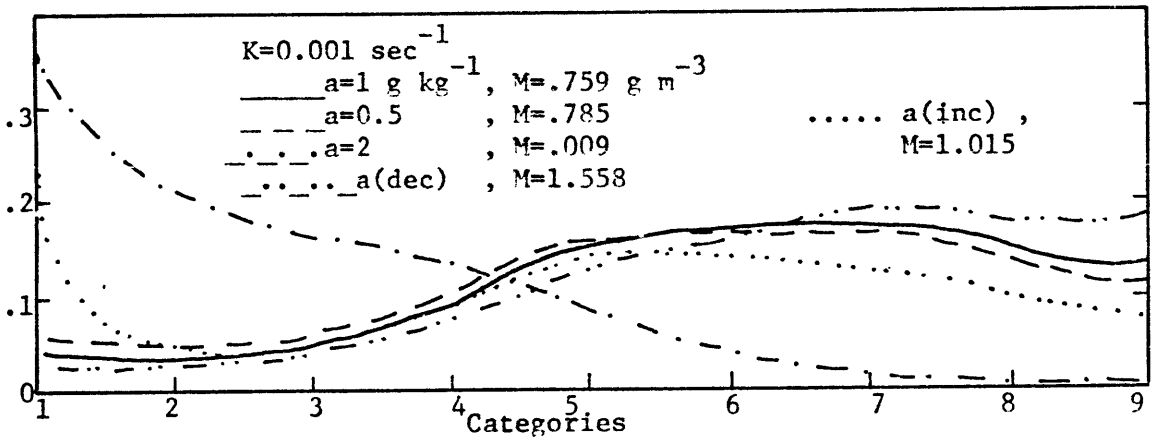

Figure 31. The computed size distribution by varying the auto-conversion threshold a, at 1000 mb and 4800 sec. in a varying updraft

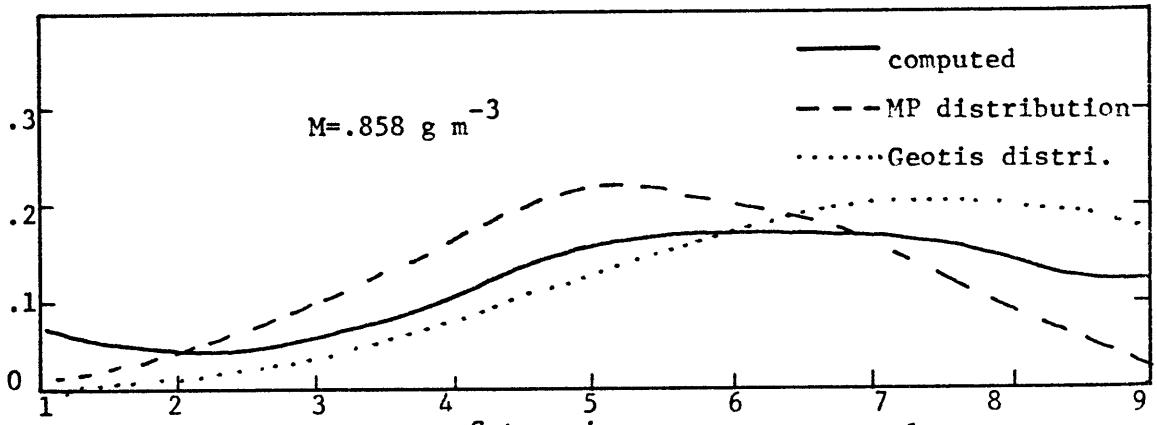

Figure 30. Same as figure 29 but with K=0.0062 sec^{-1}

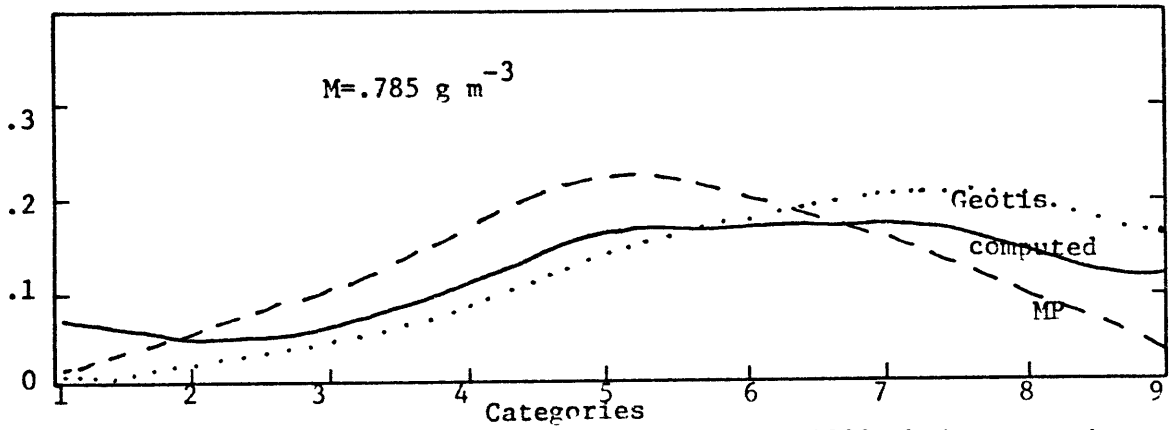

Fig. 29. Computed size distribution at 1000 mb in a varying updraft. K=0.0005 sec^{-1}. Time=4800 sec. Vertical axis represents fraction of precipitation water in each category.

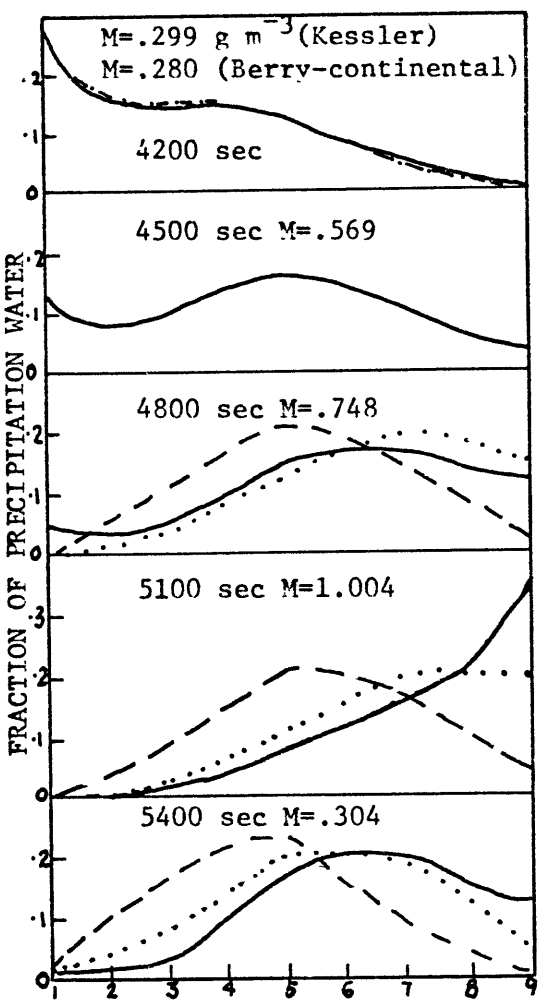

Computed (Berry AC-continental)
--- Corresponding MP distri.
-·-·- Kessler, K=0.001, a=1 g kg^{-1}
..... Geotis distribution

Figure 32. Time evolution of size distribution at 1000 mb in a varying updraft using Berry's AC for continental cloud. Results from using Kessler's AC at 4200 sec. also plotted for comparison,

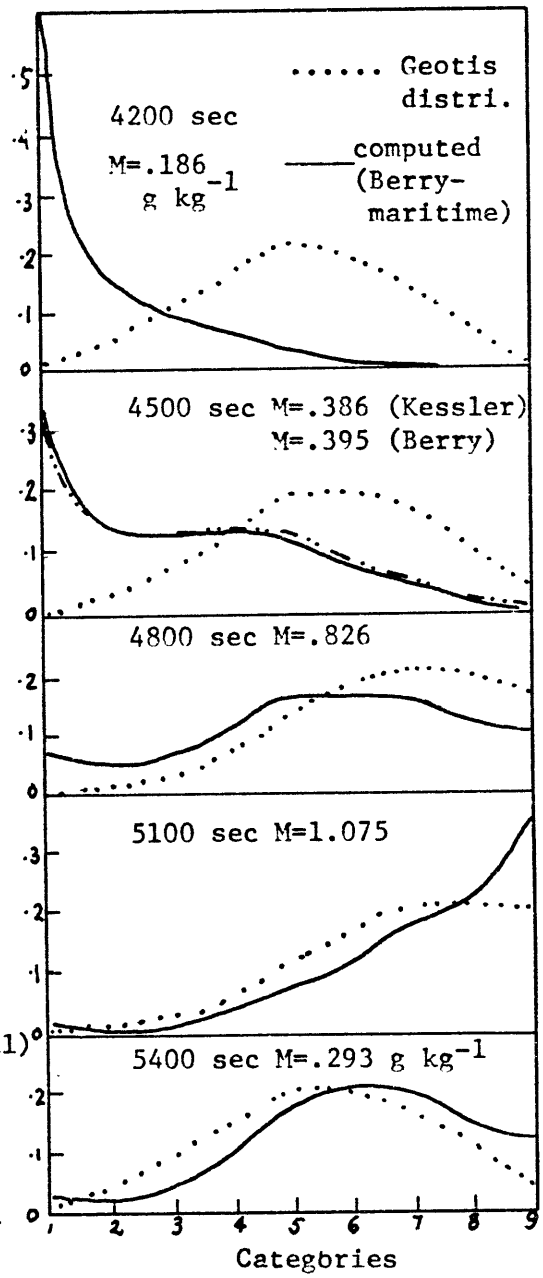

Fig. 33. Similar to fig.32 but with Berry's AC for maritime cloud. Results from using Kessler's AC with K=0.0062 sec^{-1} and a=0.5 g kg^{-1} at 4500 sec. are plotted for comparison.

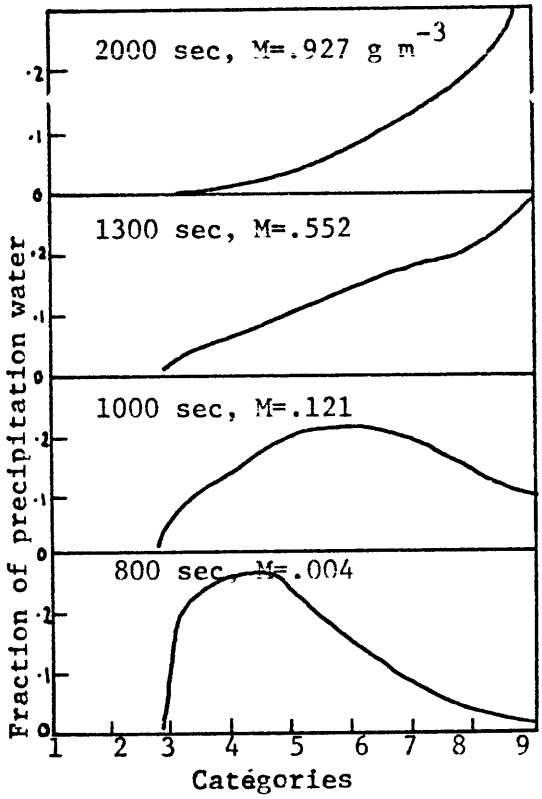

Figure 34. Time development of 'truncated distribution' in a constant updraft of -0.22 mb sec^{-1} (Kessler AC, K=0.001 sec^{-1}, a=0.5 g kg^{-1}) at 1000 mb.

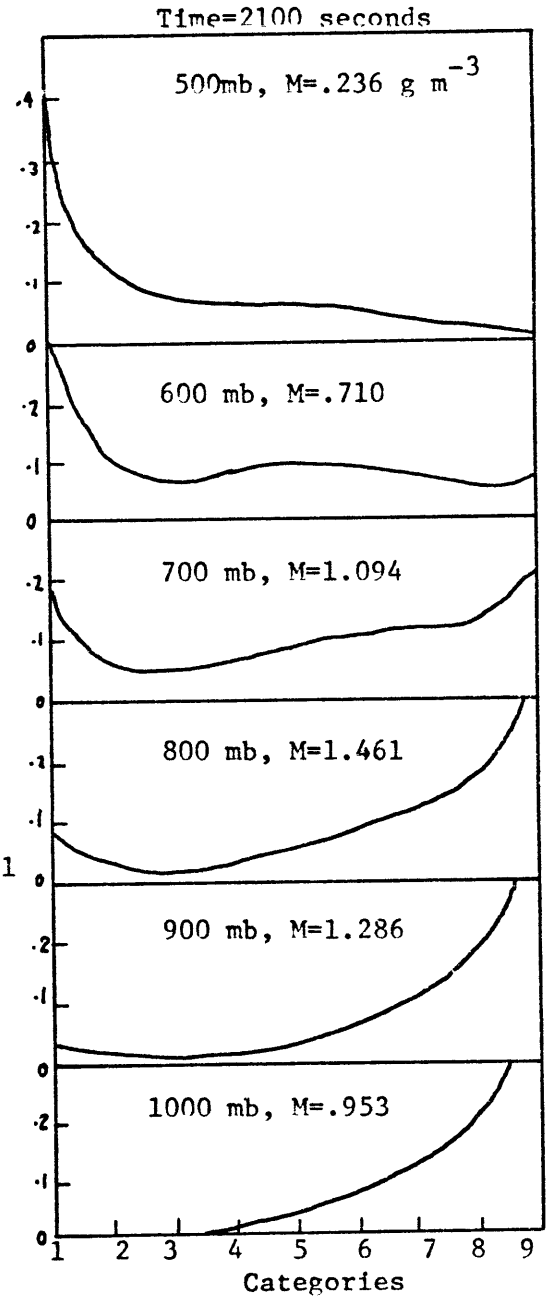

Figure. 35. Vertical variation of size distribution in a constant updraft. Conditions same as in fig. 34.

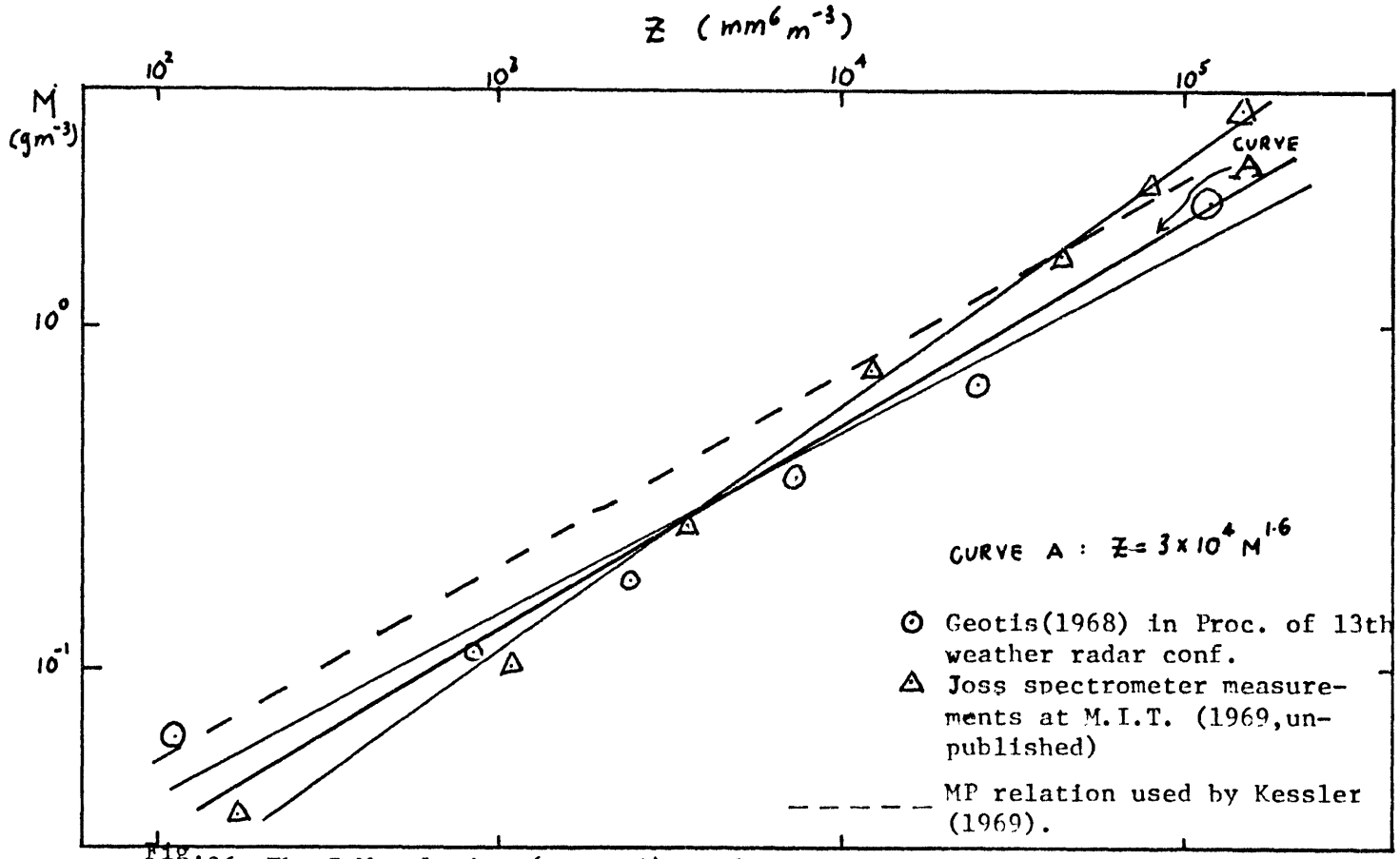

Fig. 36. The Z-M relation (curve A) used in comparison of computed reflectivity calculated from the evolved size distribution in the model.

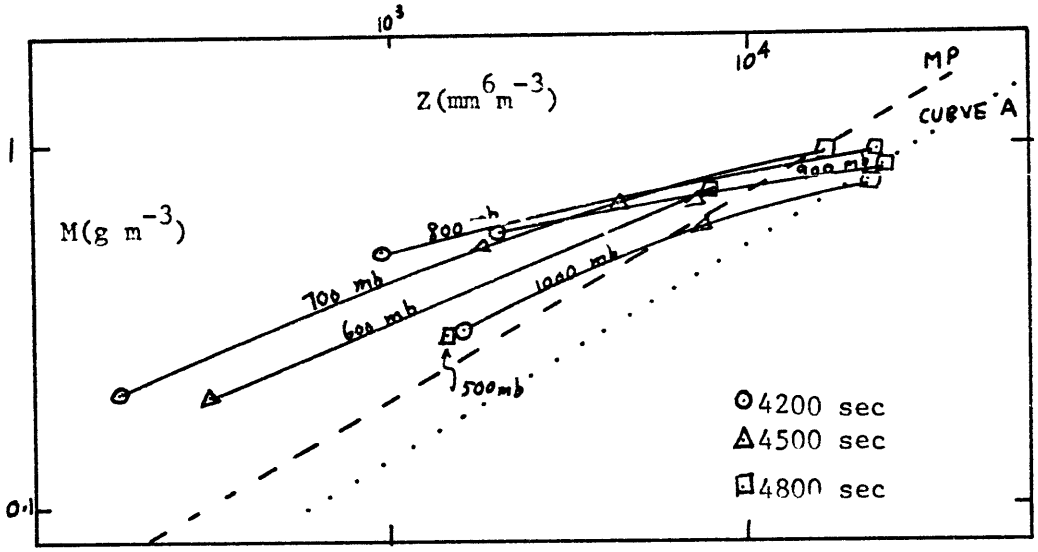

Figure 37. Time and space evolution of radar reflectivity factor computed from the different size categories before the varying updraft is turned off. Berry's AC formula for a continental cloud is used. The computed Z-M relation is shown by the solid curve.

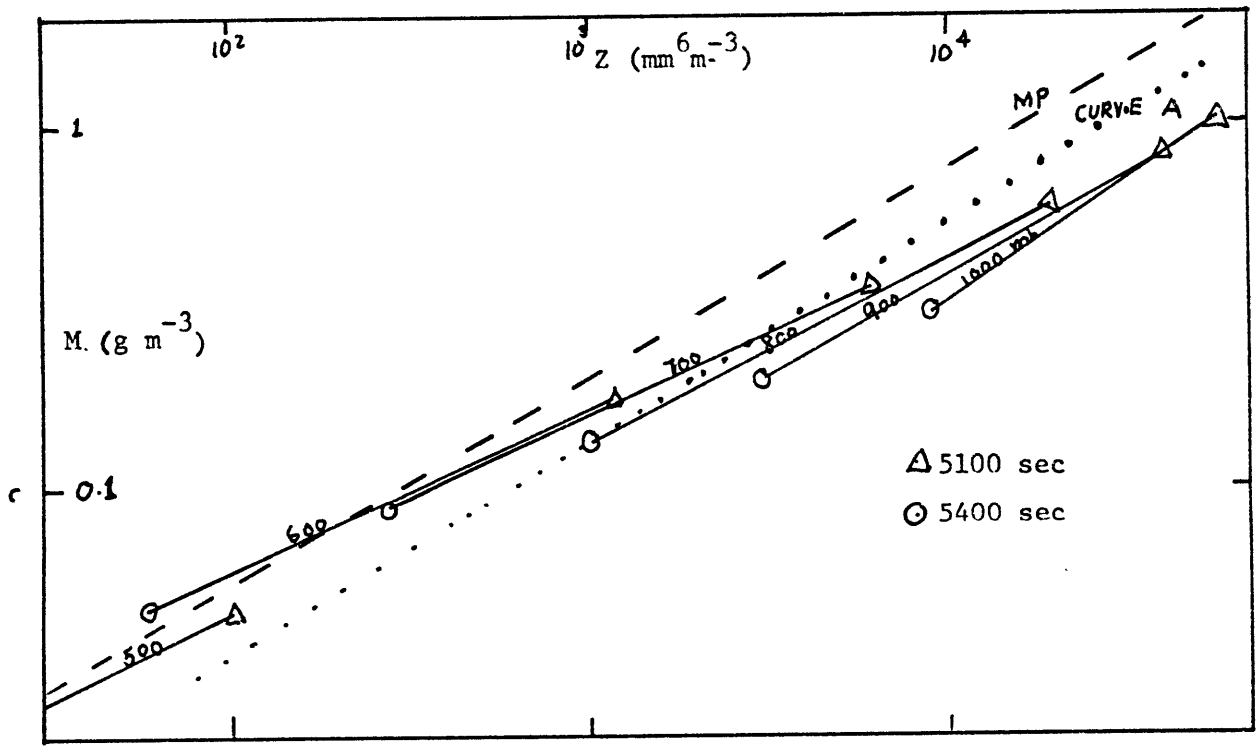

Figure. 38. Same as fig. 37. after the varying updraft is turned off.

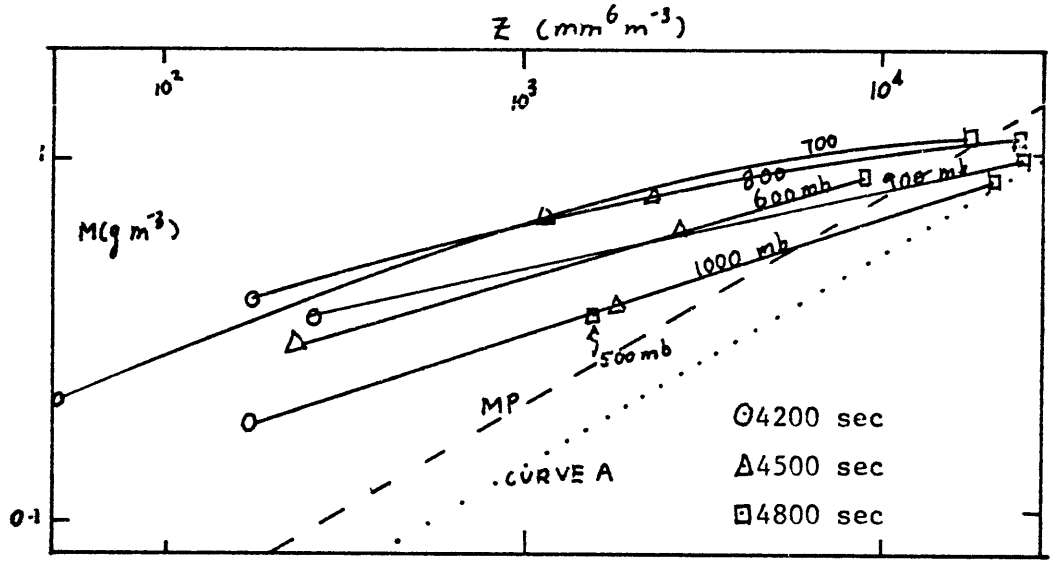

Figure 39. Same as figure 37 but using Berry' AC formula for a maritime cloud.

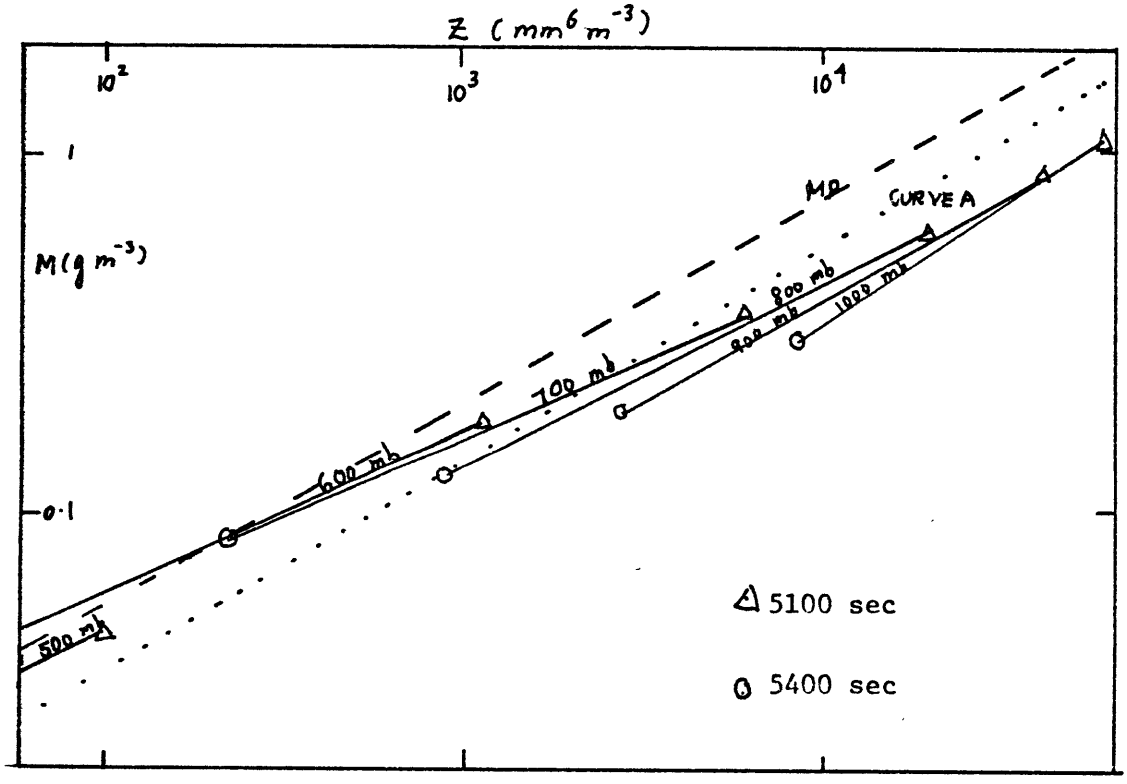

Figure 40. Same as fig ure 38 but using Berry's AC formula for a maritime cloud.

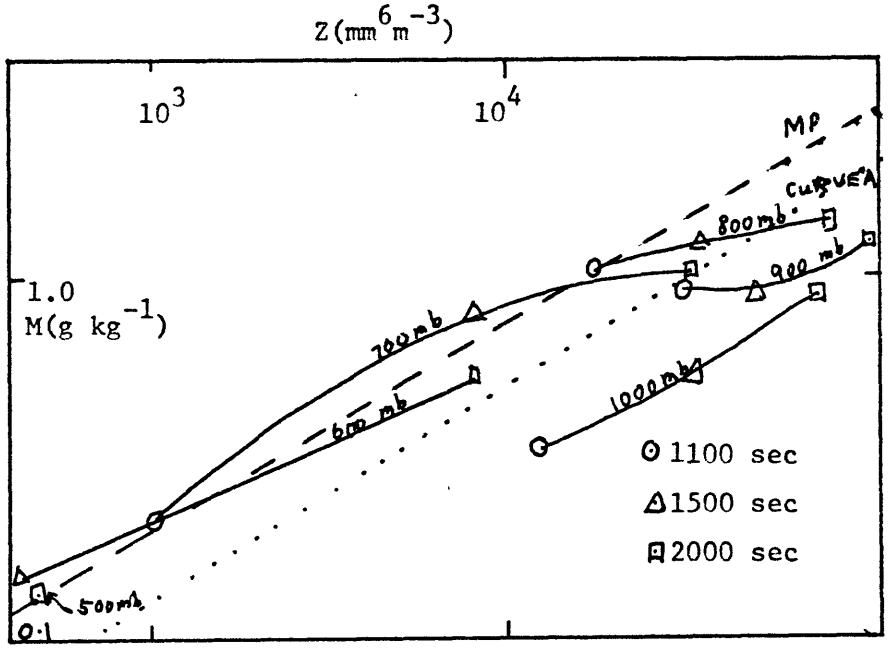

Figure. 41. Computed Z-M relation in a constant updraft of -0.22 mb sec^{-1}. Kessler's linear function with K=0.001 sec^{-1} and a=0.5 g kg^{-1} is used.

ACKNOWLEDGEMENTS

The author would like to express his sincere gratitude to Dr. Pauline M. Austin for her guidance and many valuable suggestions during the formulation of this thesis. Her kindness and encouragement have made the completion of this work possible.

Special thanks go to John Wan, who despite his busy schedule, has contributed his time in the typing of the final manuscript. The help of Mr. Steven Ricci in drafting many of the figures and Henry Wang for preparing the table of contents, list of figures and list of tables are gratefully acknowledged.

Finally the author would like to express his appreciation to the National Science Foundation who supported this work under Grant no. A27908x.

REFERENCE

Arnason, G., and R. S. Greenfield, 1972: Micro- and Macrostructures of numerically simulated convective clouds. J. Atmos. Sci., 29, 342-367.

Austin, P.M., and R.A. Houze, Jr., 1972: Analysis of the structure of precipitation patterns in New England. J. Appl. Meteor., 11, 926-935.

----- 1973: A technique for computing vertical transports by precipitating cumuli. Submitted for publication.

Berry, E.X., 1967: Cloud droplet growth by collection. J. Atmos. Sci., 24, 688-701.

_____,1968a: Modification of the warm rain process. Proc. First Natl. Conf. Wea. Modification, Boston, Amer., Meteor. Soc., 81-85

_____,1968b: A parameterization of the collection of cloud drops. Proc. Intern. Conf. Cloud Physics, Toronto, 111-114

Best, A.C., 1950: Empirical formulae for the terminal velocity of water drops falling through the atmosphere. Q.J.R.M.S., 76, 302-

Browning, K.A. 1965: A family outbreak of severe local storms- A comprehensive study of the storms in Oklahoma on 26 May 1963, Part 1, Air Force Cambridge Research Laboratories special reports, no. 32

Hyers, H.R., and Braham, R.R., 1949: The Thunderstorm, U.S. Govt. Printing Office, Washington, D.C.

Davis, M.A., and J.D. Sartor, 1967: Theoretical collision efficiencies for small cloud droplets in Stokes flow, Nature, 215, 1371-1372.

Geotis, S.G., 1968: Drop size distribution in Eastern Massachusetts, Proceedings of the Thirteenth Radar Met. Conf. 134-137.

Gunn, R., and Kinzer, G.D., 1949: The terminal velocity of fall for water droplets in stagnant air. J. of Meteor., 6, 243-248.

Hocking, L.M., 1959:The collision efficiency of small drops, Q.J.R.M.S., 85, 44-50.

Houghton, H.G., and H.E. Cramer, 1951: A theory of entrainment in convective currents. J. Meteor., 8, 95-102.

Kessler, E., 1969: On the distribution and continuity of water substance in atmospheric circulation, Meteor. Mon., Amer. Meteor. Soc., 10, 1-84.

Levine, J., 1965: The dynamics of cumulus convection in the trades. Ph.D. Thesis, Dept. of Met., MIT, Cambridge, Mass., 131 pp.

MacCready, P.B., Jr., and Takeuchi, D.M., 1968: Precipitation Initiation Mechanisms and droplet characteristics of some convective cloud core. J. Appl. Meteor., 7, 591-602.

Marshall, J.S., and W.McK. Palmer, 1948: The distribution of raindrops with size. J. Meteor., 5, 165-166.

Mason, B.J., 1969: Some outstanding problems in cloud physics--the interaction of microphysical and dynamical processes, Quart. J. Roy. Meteor. Soc., 95, 449-485.

Milne-Thomson, L.M., 1968: Theoretical Hydrodynamics, fifth edition. The Macmillan Company, 743 pp.

Newton, C.W., 1963: Dynamics of severe convective storms, in Severe Local Storms, Meteor. Mon., Amer. Meteor. Soc., 5, 33-58.

_____, 1966: Circulations in large sheared cumulonimbus, Tellus, 18, 699-713.

Ogura, Y., and T. Takahashi, 1971: Numerical simulation of the life cycle of a thunderstorm cell, Mon. Wea. Rev., 99, 895-911.

Saunders, P.M. 1962: Penetrative convection in stably stratified fluids. Tellus, 14, 177-194.

Shafrir, O., and M. Neiburger, 1963: Collision efficiencies of two spheres falling in a viscous medium, J. Geophys. Res., 68, 4141-4148.

Simpson, J., and V. Wiggert, 1969: Models of precipitating cumulus tower, Mon. Wea. Rev., 97, 471-489.

Squires, P., 1958: The microstructure and colloidal stability of warm clouds. Tellus, 10, 256-271.

Srivastava, R.C., 1967: On the role of coalescence between raindrops in shaping their size distribution. J. Atmos.Sci., 24, 287-292.

Steiner, J.T., 1972: A three dimensional numerical model of atmospheric convection. Scientific Report MW-73, McGill University.

Takeda, T., 1971: Numerical simulation of a precipitating convective cloud: the formation of a "long-lasting" cloud. J. Atmos. Sci., 28,356-376.

Weinstein, A.I., 1969: A numerical model of cumulus dynamics and microphysics. Report no. 13 to the National Sci. Found., Penn. State Univ., 75 pp.